Ab initio calculations of nuclear widths via an integral relation

Kenneth M. Nollett*
Physics Division, Argonne National Laboratory, Argonne, Illinois 60439, USA
(Received 31 May 2012; published 23 October 2012)

I describe the computation of energy widths of nuclear states using an integral over the interaction region of *ab initio* variational Monte Carlo wave functions, and I present calculated widths for many states. I begin by presenting relations that connect certain short-range integrals to widths. I then present predicted widths for $5 \leqslant A \leqslant 9$ nuclei, and I compare them against measured widths. They match the data more closely and with less ambiguity than estimates based on spectroscopic factors. I consider the consequences of my results for identification of observed states in ^{8}B, ^{9}He, and ^{9}Li. I also examine failures of the method and conclude that they generally involve broad states and variational wave functions that are not strongly peaked in the interaction region. After examining bound-state overlap functions computed from a similar integral relation, I conclude that overlap calculations can diagnose cases in which computed widths should not be trusted.

DOI: 10.1103/PhysRevC.86.044330 PACS number(s): 21.10.Tg, 21.60.De, 02.70.Ss, 27.20.+n

I. INTRODUCTION

The last decade and a half have seen enormous progress in the description of light nuclei as collections of interacting nucleons with the same properties as in vacuum [1–4]. After the formulation of potentials that fit nucleon-nucleon scattering data with high accuracy, *ab initio* calculations of nuclear structure demonstrated that the energy spectra of nuclei small enough for converged calculations (mass number $A \lesssim 12$) can be understood as arising from the vacuum nucleon-nucleon interaction [5]. The addition of a three-nucleon interaction with only two to four parameters produces quantitative agreement with experiment for the nuclear binding energies and spin-orbit splittings, including the correct ground state ($J^{\pi} = 3^{+}$ instead of 1^{+}) for ^{10}B [6].

For nuclei with $A \leqslant 4$, methods using correlated hyperspherical harmonic bases or Faddeev and similar formulations have solved bound-state, scattering, and reaction problems quite successfully [7–10]. The *ab initio* methods that have been developed for $A > 4$ nuclei are suited mainly to treatment of bound states, but there has been significant progress on unbound states in recent years. The Green's function Monte Carlo (GFMC) method has been formulated as a particle-in-a-box method and used to compute phase shifts in the ^{5}He system with a full realistic Hamiltonian [11]. The no-core shell model (NCSM) has been merged with the resonating group method (RGM) to produce phase shifts and reaction cross sections in several systems using effective two-body forces without explicit three-body terms [12–15]. The coupled-cluster method has been combined with a Gamow shell-model basis to compute complex energies $E = E_R - i\Gamma/2$ of resonances and thus their excitation energies E_R and total widths Γ. It has been applied to resonances of He isotopes and $A = 17$ nuclei, but it has not been used to produce cross sections [16,17]. All of these approaches to scattering are computationally challenging, and significant human and computer effort is required for each individual system.

Even before the development of true scattering and reaction calculations in $A > 4$ nuclei, there were accurate energy calculations for many unbound resonance states [1,3], produced by approximating them with bound (i.e., square-integrable) wave functions and real energies. This approach is successful for states sufficiently narrow that important features of their structure can be accommodated within the model space. One way to understand these calculations is as approximations to Gamow's decaying complex-energy states [18] with energies near the real axis (i.e., small widths).

Quantum Monte Carlo (QMC) calculations of square-integrable "pseudobound" states begin with a variational Monte Carlo (VMC) calculation, in which a complicated but closed-form wave function containing large amounts of correlation is produced by minimizing the energy expectation value with respect to many variational parameters [1]. The computational effort in the VMC method lies in computing energy expectation values by Monte Carlo integration over all particle coordinates, and a square-integrable wave function is necessary for both energy and normalization integrals to converge. The variational ansatz incorporates square integrability through particle correlations that decay exponentially at large separation, and reasonable energies result because the long-range tails of the true resonant wave function have small amplitudes relative to the "interaction region" where all nucleons interact.

The second step in application of the QMC method to nuclei is a GFMC calculation. This step also requires square-integrable wave functions for evaluation of matrix elements. GFMC takes the VMC wave function as a starting point and evolves the Schrödinger equation for imaginary values of the time $t = i\tau$ through a series of small steps. This evolution filters high-energy contamination out of the wave function and for large τ leaves behind the lowest-energy eigenstate contained in the VMC starting point. For bound or narrow states, this procedure "converges" at large τ to a unique energy [6,19,20]. For broad states the GFMC propagation drifts slowly toward the lowest available threshold; even in

*Present address: Department of Physics and Astronomy, Ohio University, Athens, OH 45701; nollett@ohio.edu.

very long GFMC propagations, the curve of energy versus τ for such states fails to flatten out at a "converged" energy. Presumably this also occurs for the narrow states, but with a decline too slow to have been noticed in calculations so far.

Because the calculated energies of narrow resonances in the QMC methods are believed to be accurate, it is natural to ask whether widths could be extracted from these calculations, avoiding the considerable effort of explicit scattering and reaction calculations. Attempts to correlate the width with the rate of decline of the energy, $dE/d\tau$, in the late-time GFMC propagation failed, so the rate may depend more on the starting wave function than on the physical width [21].

Even in explicit scattering calculations, some widths are effectively too narrow to resolve by QMC methods. Direct QMC calculations of widths so far consist of energy calculations for a series of specified boundary conditions [11], so the smallest width that can be computed must be larger than the energy resolution of the method. As an extreme example, the ground state of ^{9}B has a total energy of -56.3 MeV and a width of 0.5 keV, roughly 0.01% of the total. Since the typical precision claimed for GFMC energy calculations is 1%, this width will not be amenable to calculation in this way.

Here I present a method to extract approximate widths from QMC wave functions. The basis of this approach is a relation between the partial width in a specified breakup channel and an integral over the "interaction region" where all of the nucleons are close to each other. This relation has been used in the literature, though not (to my knowledge) in explicit application to many-body wave functions. It has been used particularly in models of α [22,23] and proton [24–29] decays of heavy nuclei in order to avoid direct integration of the Schrödinger equation to impractically large radii. It is also closely related to Green's function formulations of scattering theory. There has been considerable interest in applying such formulations to *ab initio* calculations in the recent literature: they have been used to extract asymptotic normalization coefficients (ANCs) from many-body bound states computed in various approximations [30–33] and are coming into wider use for scattering problems [8,34–38]. Preparation for future reaction calculations of that kind is a primary motivation of the present work.

Although the integral relation can be used to compute the partial width in any two-body decay channel if wave functions of the parent and daughter nuclei are known, I confine my consideration in the present study to nucleon emission. I compute widths for all narrow ($\Gamma \lesssim 1$ MeV) one-nucleon decays to bound states in $5 \leqslant A \leqslant 9$ nuclei. I also present results for several specific broad states for which better theoretical information concerning widths would be useful and for some with unbound final states that are well represented by pseudobound wave functions.

The integral relation applied here can be used with either GFMC or VMC wave functions, extending even to use of the same computer routines. Application to GFMC requires more computation and additional bookkeeping, so I have chosen in this initial study to use only VMC wave functions. This work represents the extension to unbound states of the methods presented in Ref. [33]. The integral relation used here may be used with other many-body methods, but it is particularly well suited to QMC wave functions because of its formulation as a short-range integral and because of the transparent treatment of fermion antisymmetry in the QMC methods.

The remainder of this paper is organized as follows: In Sec. II I motivate and define the integral method, and I discuss its accuracy and its connection to overlap calculations. In Sec. III I describe the application of the integral method to VMC wave functions. In Sec. IV I present the results of calculations for specific states, compare computed and experimental widths, and consider how accurately widths may be computed from spectroscopic factors. Along the way I present overlap calculations of VMC wave functions that are likely to be improvements over previous calculations and may prove useful for treatment of transfer reactions. Finally, in Sec. V I summarize my results and briefly mention future directions for this work.

II. AN INTEGRAL RELATION FOR RESONANCE WIDTHS

A. The connection between widths and asymptotic normalizations

Consider a many-body wave function Ψ at energy E above the threshold for breakup into clusters 1 and 2 that have wave functions ψ_1 and ψ_2, respectively, and no internal angular momentum. Assume also for the moment that only this breakup channel is open. Since ψ_1 and ψ_2 are spinless, the orbital angular momentum l of their motion is equal to the total angular momentum J of Ψ. Given appropriate boundary conditions, Ψ at large separations r_{12} of the clusters is a linear combination of an incoming wave proportional to $I_l(\eta, kr_{12})/r_{12}$ and an outgoing wave proportional to $O_l(\eta, kr_{12})/r_{12}$, each normalized to probability flux $\hbar k/\mu$ in its appropriate direction at $r_{12} \to \infty$. (For all special functions, I follow the conventions of Refs. [39] and [40].) These functions depend on the energy E through the wave number $k \equiv \sqrt{2\mu E}/\hbar$, where μ is the reduced mass of the clusters, and through the Sommerfeld parameter $\eta \equiv Z_1 Z_2 e^2 \mu/\hbar k$, where Z_1 and Z_2 are the charge numbers of the clusters. O_l and I_l solve the radial Coulomb-Schrödinger equation

$$-\frac{d^2 u_l}{d\rho^2} + \left(\frac{l(l+1)}{\rho^2} + \frac{2\eta}{\rho}\right) u_l = u_l, \tag{1}$$

with $\rho = kr_{12}$ and outward and inward flux, respectively, at $r_{12} \to \infty$. In terms of I_l and O_l, Ψ (assumed to have angular-momentum projection m, omitted from subsequent expressions) is

$$\Psi(r_{12} \to \infty) = C_l \psi_1 \psi_2 Y_{lm}(\hat{\mathbf{r}}_{12})[I_l(\eta, kr_{12}) - S_l(k) O_l(\eta, kr_{12})]/r_{12}, \tag{2}$$

where $Y_{lm}(\hat{\mathbf{r}}_{12})$ is a spherical harmonic. In this single-channel case with both incoming and outgoing waves, the normalization C_l is arbitrary. If k and η are real, conservation of probability guarantees that the effect of scattering is to multiply the outgoing wave O_l by a complex phase factor relative to the incoming wave I_l, so that the function $S_l(k)$ may be written in terms of a real phase shift $\delta_l(k)$ as $S_l = e^{2i\delta_l}$. The function $S_l(k)$ is the single-channel case of the S matrix, which gives the amplitude and phase of outgoing waves in terms

of specified ingoing amplitudes, and it determines the cross section uniquely.

Resonances in the scattering of clusters 1 and 2 occur at real energies near poles of $S_l(k)$ and produce peaks in the scattering cross section where $\tan\delta_l \simeq \Gamma/(E - E_R)$ around some resonance with energy E_R and width Γ. S-matrix poles in general occur at complex k (and thus complex E). It is evident from Eq. (2) that at such a pole the wave function takes the form

$$\Psi(r_{12} \to \infty) = C_l' \psi_1 \psi_2 Y_l(\hat{\mathbf{r}}_{12}) O_l(\eta, kr_{12})/r_{12}, \tag{3}$$

with only outgoing flux. This is the same sort of decaying complex-energy state originally formulated in Gamow's treatment of α decay [18]. The probability flux out of this state is $\hbar k|C_l'|^2/\mu$, so the normalization constant is no longer arbitrary but carries information about the size of the outgoing flux relative to the total wave function. If Ψ has been normalized to unit total probability in some finite region, its lifetime is inversely proportional to the outward probability flux. By writing Ψ in the form

$$\Psi(r_{12} \to \infty) = C_l' \psi_1 \psi_2 Y_l(\hat{\mathbf{r}}_{12})[[S_l(k)]^{-1} I_l - O_l]/r_{12}, \tag{4}$$

and defining Ψ to have unit norm in some regularization scheme, it can be shown that the residue of the S-matrix pole is proportional both to the squared normalization constant $|C_l'|^2$ and to the imaginary part of the pole energy [41–43]. The relations among $|C_l'|^2$, the lifetime, and the pole location imply that the width $\Gamma = \hbar^2 k|C_l'|^2/\mu$. (Derivations that deal rigorously with the normalization of Ψ may be found in Refs. [41,42].) The width may thus be computed from the normalization constant C_l'.

Physically realized systems have real energies, so formulation of the width in terms of complex-energy Gamow states is often inconvenient. For the QMC methods, not only is the energy real, but the wave functions are stationary waves, being the sums of incoming and outgoing waves with zero total flux in each channel. Assuming again a single open channel of given angular momentum, a standing-wave solution is asymptotically

$$\Psi(r_{12} \to \infty) = C_l \psi_1 \psi_2 Y_l(\hat{\mathbf{r}}_{12})[F_l(\eta, kr_{12}) + K_l(k) G_l(\eta, kr_{12})]/r_{12}, \tag{5}$$

for some different C_l than before. $F_l(\eta, kr_{12})$ is the regular Coulomb function that satisfies $F_l(\eta, 0) = 0$, $G_l(\eta, \rho)$ satisfies the Wronskian relation

$$\frac{dF_l(\eta,\rho)}{d\rho} G_l(\eta,\rho) - F_l(\eta,\rho)\frac{dG_l(\eta,\rho)}{d\rho} = 1,$$

and the two are related to O_l and I_l by

$$O_l(\eta,\rho) = G_l(\eta,\rho) + iF_l(\eta,\rho), \tag{6}$$

$$I_l(\eta,\rho) = G_l(\eta,\rho) - iF_l(\eta,\rho). \tag{7}$$

The function $K_l(k)$ is the single-channel case of the K matrix. Equations (2), (6), and (7) combine to give

$$K_l(k) = i\frac{1 - S_l(k)}{1 + S_l(k)} \tag{8}$$

so that $K_l(k) = \tan\delta_l(k)$. Equation (5) may then be written as

$$\Psi(r_{12} \to \infty) = C_l' \psi_1 \psi_2 Y_l(\hat{\mathbf{r}}_{12})[\cos\delta_l F_l(\eta, kr_{12}) + \sin\delta_l G_l(\eta, kr_{12})]/r_{12} \tag{9}$$

for some C_l' determined by an appropriate normalization of Ψ. At a resonance, $\delta_l = \pi/2$ and $d\delta_l/dE > 0$. This corresponds to a pole of $K_l(k)$ on the positive real axis, so that

$$\Psi(r_{12} \to \infty) = C_l' \psi_1 \psi_2 Y_l(\hat{\mathbf{r}}_{12}) G_l(\eta, kr_{12})/r_{12} \tag{10}$$

$$= \tfrac{1}{2} C_l' \psi_1 \psi_2 Y_l(\hat{\mathbf{r}}_{12})[I_l(\eta, kr_{12}) + O_l(\eta, kr_{12})]/r_{12}. \tag{11}$$

The standing-wave solution at resonance is thus the sum of equal inward and outward fluxes, each of magnitude $\hbar k|C_l'|^2/4\mu$. This is the rate at which Ψ decays through the outgoing wave and is replenished by the ingoing wave. In analogy with the complex-energy case, it can be shown that the residue of the K matrix at the resonance pole is proportional to $|C_l'|^2$ for a wave function normalized to unity in a finite region [44–46], up to corrections arising from the choice of normalization volume. These corrections are small as long as the wave function has a much smaller amplitude in the asymptotic region than in the interaction region [42,44,45], as is expected for a long-lived resonance state. After comparing Eqs. (3) and (10), it is unsurprising that the result of a rigorous derivation is $\Gamma \approx \hbar^2 k|C_l'|^2/\mu$.

I have sketched the considerations that lead to the connection between resonance width and wave function asymptotic normalization for the case of a single open channel and spinless daughter nuclei. These considerations carry over directly to *ab initio* wave functions, but it is necessary to account for complications absent from the toy model.

Most complications of the *ab initio* case amount to additional bookkeeping implied by multiple final-state channels, antisymmetry of the wave function, and daughters with nonzero angular momenta. Multiple types of decay products may be emitted, and their nonzero internal angular momenta may couple in multiple ways. The simple right-hand sides of Eqs. (2) and (5) are replaced by sums over all breakup and l channels of a given total angular momentum J and parity π. The formalism to describe multichannel wave functions in this case may be found in many treatments of reaction theory (e.g., Refs. [40,45,47,48]). The coefficient $S_l(k)$ in Eq. (2) is replaced by a matrix S_{ab} that gives the outgoing flux in channel a produced by unit incoming flux in channel b, and $K_l(k)$ in Eq. (5) is similarly replaced by a matrix K_{ab} that gives the irregular-function amplitude in channel a produced by unit regular-function amplitude in channel b. If the initial state in a reaction problem has amplitude x_a in channel a, then

$$\Psi(\text{all } r_a \to \infty) = \sum_a \mathcal{A}_a\left[\psi_{a1}^{J_{a1}}\left[\psi_{a2}^{J_{a2}} Y_{l_a}(\hat{\mathbf{r}}_a)\right]_{j_a}\right]_J \times \left\{x_a F_{l_a}(\eta_a, k_a r_a) + y_a G_{l_a}(\eta_a, k_a r_a)\right\}/r_a. \tag{12}$$

In this expression, channel a is characterized by daughter nuclei with wave functions $\psi_{a1}^{J_{a1}}$ and $\psi_{a2}^{J_{a2}}$, wave number k_a, Sommerfeld parameter η_a, and daughter separation r_a. The

orbital angular momentum of this channel is l_a, and the square brackets denote coupling of the daughter angular momenta J_{a2} and l_a first to "jj-coupled" angular momentum j_a and then with J_{a2} to form total angular momentum J. (The use of this coupling anticipates its later utility in defining channels in QMC wave functions.) The antisymmetrization operator $\mathcal{A}_a$ carries out an antisymmetric sum over all partitions of nucleons into daughters $a1$ and $a2$ with mass numbers A_1 and A_2 and multiplies by the normalization $\sqrt{A_1!A_2!/A!}$. The index a is taken to specify the daughter nuclei as well as the channel quantum numbers j_a, J_{a1}, J_{a2}, l_a, and π_a.

Away from resonance, the irregular-function amplitudes are given by $y_a = \sum_b K_{ab} x_b$. At a pole of K_{ab}, all asymptotic channels that are coupled to the resonance have wave functions proportional to $G_{l_a}(\eta_a, k_a r_a)$. Then the corresponding x_a are irrelevant and may be set to zero. If Ψ at a pole is normalized to unit probability within some finite volume that includes the whole interaction region, the residue of K_{aa} is proportional to $|y_a|^2$ [44,45]. The partial width of the resonance in channel a is proportional to this residue, just as it was in the single-channel case discussed above [46,48]. It can be shown that the imaginary part of the corresponding S-matrix pole energy is proportional to the sum of these partial widths [48], so the pole residues give the partial widths, whereas the S-matrix pole location gives only the total width.

The channel radial functions defined by the summed terms in Eq. (12) can be isolated from Ψ by projecting it onto the channel functions

$$\Phi_a(\boldsymbol{\xi}_{a1}, \boldsymbol{\xi}_{a2}, \mathbf{r}_a) \equiv \mathcal{A}_a \tilde{\Phi}_{a,p}(\boldsymbol{\xi}_{a1}, \boldsymbol{\xi}_{a2}, \mathbf{r}_a), \tag{13}$$

where the channel function in a given partition p of the nucleons into clusters is

$$\tilde{\Phi}_{a,p}(\boldsymbol{\xi}_{a1}, \boldsymbol{\xi}_{a2}, \mathbf{r}_a) \equiv \left[\psi_{a1}^{J_{a1}}\left(\boldsymbol{\xi}_{a1}^{p}\right)\left[\psi_{a2}^{J_{a2}}\left(\boldsymbol{\xi}_{a2}^{p}\right) Y_{l_a}(\hat{\mathbf{r}}_a)\right]_{j_a}\right]_J, \tag{14}$$

$$\boldsymbol{\xi}_{ai} = \boldsymbol{\xi}_{ai}^{p} \equiv \{\mathbf{r}_j - \mathbf{r}_{ai}\}, \quad j \in ai. \tag{15}$$

The $\boldsymbol{\xi}_{ai}$ are the internal coordinates of $\psi_{ai}^{J_{ai}}$, written in terms of nucleon coordinates in the specified partition p as differences $\boldsymbol{\xi}_i^p$ of the coordinates $\mathbf{r}_j$ of nucleons within daughter i and the center of mass of daughter i. The daughter centers of mass $\mathbf{r}_{ai}$ are related to their separation $\mathbf{r}_a$ by

$$\mathbf{r}_{a2} - \mathbf{r}_{a1} = \mathbf{r}_a, \tag{16}$$

$$A_1 \mathbf{r}_{a1} + A_2 \mathbf{r}_{a2} = 0. \tag{17}$$

Using bracket notation to indicate inner product in nucleon spin-isospin space and integration over all nucleon coordinates $\mathbf{R} = \{\mathbf{r}_j\}$, we have

$$\begin{aligned}\langle \Phi_a | \frac{\delta(r_a - r)}{r_a^2} | \Psi \rangle &= \sqrt{\frac{A_1!A_2!}{A!}} \sum_p (-1)^p \int \left[\psi_{a1}^{J_{a1}}\left(\boldsymbol{\xi}_{a1}^{p}\right)\left[\psi_{a2}^{J_{a2}}\left(\boldsymbol{\xi}_{a2}^{p}\right) Y_{l_a}(\hat{\mathbf{r}}_a)\right]_{j_a}\right]_J^{\dagger} \\ &\quad \times \frac{\delta(r_a - r)}{r_a^2} \Psi d^{3A} R,\end{aligned} \tag{18}$$

which for an exact solution of the Hamiltonian gives the overlap function

$$R_a(r) \equiv \langle \Phi_a | \delta(r_a - r) | \Psi \rangle / r^2 \tag{19}$$

$$\underset{r\to\infty}{=} \left\{x_a F_{l_a}(\eta_a, k_a r) + y_a G_{l_a}(\eta_a, k_a r)\right\}/r. \tag{20}$$

It is this function that multiplies the daughter wave functions in Eq. (12). [Formally, the integral in Eq. (18) extends over only $3(A-1)$ coordinates, because center-of-mass motion is irrelevant. The wave functions used in nuclear QMC calculations are translationally invariant, allowing the integral to be written as extending over all coordinates; the effect of center-of-mass motion cancels out when dividing computed quantities by the wave function normalization.]

B. Integral relations and asymptotic normalizations

Equation (10) suggests that the partial width of a real-energy resonance state may be found by first computing Ψ at resonance and then projecting onto the desired channel and dividing by G_l/r to obtain the partial width

$$\Gamma_a = \frac{\hbar k_a}{\mu_a} \left| \frac{R_a(r) r}{G_l(\eta_a, k_a r)} \right|^2. \tag{21}$$

This approach is useful when Ψ can be computed accurately in the large-r region (as in Ref. [43]). However, it often happens that Ψ is computed accurately in the interaction region, but computation in the asymptotic region described by Eq. (12) is difficult or inconvenient.

A more robust approach proceeds through a Green's function formalism. One begins with the Schrödinger equation,

$$(H - E)\Psi = 0, \tag{22}$$

with H the Hamiltonian operator and E the energy. To isolate a particular channel a, as defined above, it is useful to choose a partition p of nucleons into the daughter nuclei in that channel and write H as a sum of parts internal to the daughters and parts that depend on their relative motion. Working in the center-of-mass frame, we have

$$H = T_{a,p} + U_{\text{rel}}^{a,p} + H_1^{a,p} + H_2^{a,p} + V_C^a - V_C^a, \tag{23}$$

where $T_{a,p}$ is the kinetic energy of relative motion of the daughters. The operator $H_i^{a,p}$ is the part of the Hamiltonian (kinetic plus potential) involving only the coordinates $\boldsymbol{\xi}_{ai}^p$ within daughter i. $U_{\text{rel}}^{a,p}$ contains the remaining terms of the potential, consisting of interactions between nucleons in daughter 1 and nucleons in daughter 2:

$$U_{\text{rel}}^{a,p} = \sum_{i\in a1; j\in a2} v_{ij} + \frac{1}{2} \sum_{i\in a1; j,k\in a2} V_{ijk} + \frac{1}{2} \sum_{i,j\in a1; k\in a2} V_{ijk}, \tag{24}$$

This is *not* an effective interaction but rather the sum of all terms of the many-body potential (with two-body terms v_{ij} and three-body terms V_{ijk}) linking the two daughters.

The point-Coulomb interaction between daughters, $V_C^a(r_a) = Z_{a1}Z_{a2}e^2/r_a$, is added and subtracted for reasons that will become apparent later; it is zero if one of the daughters is a neutron.

The energy E may be similarly broken up into the sum of the daughter internal energies E_{ai} and the channel energy E_a:

$$E = E_{a1} + E_{a2} + E_a. \tag{25}$$

Then Eq. (22) becomes

$$\begin{aligned}\big(T_{a,p} + U_{\rm rel}^{a,p} + V_C^a - V_C^a + H_1^{a,p} \\ + H_2^{a,p} - E_{a1} - E_{a2} - E_a\big)\Psi = 0.\end{aligned} \tag{26}$$

Rearranging terms and multiplying by the operator $[T_{a,p} + V_C^a - E_a]^{-1}$, we find

$$\begin{aligned}\Psi = &-\big[T_{a,p} + V_C^a - E_a\big]^{-1}\big(U_{\rm rel}^{a,p} - V_C^a\big)\Psi \\ &-\big[T_{a,p} + V_C^a - E_a\big]^{-1}\big(H_1^{a,p} + H_2^{a,p} - E_{a1} - E_{a2}\big)\Psi.\end{aligned} \tag{27}$$

The next step is to project Ψ onto channel a, as in Eq. (19). Projection of Eq. (27) onto a channel function $\tilde{\Phi}_{a,p}$ of Eq. (14) gives

$$\begin{aligned}&\big[\tilde{\Phi}_{a,p}\big(\boldsymbol{\xi}_1^p, \boldsymbol{\xi}_2^p, \mathbf{r}_a'\big)\big]^\dagger\Psi \\ &\quad= -[\tilde{\Phi}_{a,p}(\mathbf{r}_a')]^\dagger\big[T_{a,p} + V_C^a - E_a\big]^{-1}\big(U_{\rm rel}^{a,p} - V_C^a\big)\Psi \\ &\qquad-[\tilde{\Phi}_{a,p}(\mathbf{r}_a')]^\dagger\big[T_{a,p} + V_C^a - E_a\big]^{-1} \\ &\qquad\times\big(H_1^{a,p} + H_2^{a,p} - E_{a1} - E_{a2}\big)\Psi\end{aligned} \tag{28}$$

(where we abbreviate $\tilde{\Phi}_{a,p}$ on the right side by omitting the cluster internal coordinates), but since

$$\big(H_i^{a,p} - E_{ai}\big)\psi_{ai}^{J_a}\big(\boldsymbol{\xi}_i^p\big) = 0,$$

the second term in the right side of Eq. (28) is zero, and

$$\begin{aligned}&[\tilde{\Phi}_{a,p}(\mathbf{r}_a')]^\dagger\Psi \\ &\quad= -[\tilde{\Phi}_{a,p}(\mathbf{r}_a')]^\dagger\big[T_{a,p} + V_C^a - E_a\big]^{-1}\big(U_{\rm rel}^{a,p} - V_C^a\big)\Psi.\end{aligned} \tag{29}$$

Now, the operator $[T_{a,p} + V_C^a - E_a]^{-1}$ takes functions of nucleon coordinates $\mathbf{R}$ to functions of nucleon coordinates $\mathbf{R}'$ with different values of the separation $\mathbf{r}_a$ but with the $\boldsymbol{\xi}_i^p$ untouched. Its application to a function $\phi_1(\mathbf{R})$ and projection onto a second function $\phi_2(\mathbf{R}')$ may be written as an integral over a Green's function that contains a product of Coulomb wave functions:

$$\phi_2^\dagger(\mathbf{R}')\big[T_{a,p} + V_C^a - E_a\big]^{-1}\phi_1(\mathbf{R}) = \frac{2\mu}{\hbar^2 k_a}\phi_2^\dagger(\mathbf{R}')\int d^3r_a\,\frac{F_{l_a}(\eta_a, k_a r_<)G_{l_a}(\eta_a, k_a r_>)}{r_< r_>}Y_{l_a}(\hat{\mathbf{r}}_a')Y_{l_a}^*(\hat{\mathbf{r}}_a)\phi_1(\mathbf{R}), \tag{30}$$

following the usual notation that $r_<$ denotes the smaller of r_a (a Jacobi coordinate specified for partition p by $\mathbf{R}$) and r_a' (specified by p and $\mathbf{R}'$), while $r_>$ denotes the larger of r_a and r_a'. By rewriting Eq. (18) in terms of Eq. (29) and applying Eq. (30), the result of integration over $\mathbf{r}_a'$ and antisymmetrization over partitions p is

$$\begin{aligned}\langle\Phi_a|\frac{\delta(r_a - r)}{r_a^2}|\Psi\rangle = -\frac{2\mu}{\hbar^2 k_a}\Bigg[&\frac{G_{l_a}(\eta_a, k_a r)}{r}\mathcal{A}_a\int_{r_a<r}\frac{F_{l_a}(\eta_a, k_a r_a)}{r_a}[\tilde{\Phi}_{a,p}(\mathbf{r}_a)]^\dagger\big(U_{\rm rel}^{a,p} - V_C^a\big)\Psi\, d^{3A}R \\ &+\frac{F_{l_a}(\eta_a, k_a r)}{r}\Bigg\{B_{a,\infty} + \mathcal{A}_a\int_{r_a>r}\frac{G_{l_a}(\eta_a, k_a r_a)}{r_a}[\tilde{\Phi}_{a,p}(\mathbf{r}_a)]^\dagger\big(U_{\rm rel}^{a,p} - V_C^a\big)\Psi\, d^{3A}R\Bigg\}\Bigg].\end{aligned} \tag{31}$$

The constant of integration $B_{a,\infty}$ can be determined from Ψ as in Refs. [36,38]; as discussed below, $B_{a,\infty} = 0$ at resonance. Finally, I denote the integrals in Eq. (31) by

$$B_a(r) = \frac{2\mu}{\hbar^2 k_a}\mathcal{A}_a\int_{r_a>r}\frac{G_{l_a}(\eta_a, k_a r_a)}{r_a}[\tilde{\Phi}_{a,p}(\mathbf{r}_a)]^\dagger\big(U_{\rm rel}^{a,p} - V_C^a\big)\Psi\, d^{3A}R, \tag{32}$$

$$C_a(r) = \frac{2\mu}{\hbar^2 k_a}\mathcal{A}_a\int_{r_a<r}\frac{F_{l_a}(\eta_a, k_a r_a)}{r_a}[\tilde{\Phi}_{a,p}(\mathbf{r}_a)]^\dagger\big(U_{\rm rel}^{a,p} - V_C^a\big)\Psi\, d^{3A}R, \tag{33}$$

so that

$$R_a(r) = -\{[B_{a,\infty} + B_a(r)]F_l(\eta_a, k_a r) + C_a(r)G_l(\eta_a, k_a r)\}/r. \tag{34}$$

Many derivations of Eq. (34) and equivalent (through analytic continuation) bound-state expressions may be found in the literature (e.g., Refs. [36,47,49,50]).

Several observations may be made at this point. The choice to add and subtract the point-Coulomb interaction V_C^a in Eq. (23) has two important consequences. First, it guarantees that the overlap $R_a(r \to \infty)$ computed from Eq. (34) is a linear combination of F_l and G_l, as required for solutions of the Schrödinger equation governing Ψ. Second, the nuclear interaction is short-ranged, so that, at large separations, the interaction between daughter nuclei is dominated by the monopole term of their Coulomb interaction. Since this is

just equal to V_C^a, the difference $(U_{\rm rel}^{a,p} - V_C^a)$ goes rapidly to zero for r beyond the range of the nuclear interaction. For the interactions and wave functions discussed below, this typically happens at $r \simeq 7$ fm. Thus, $B_a(r \gtrsim 7\ {\rm fm}) \sim 0$, and $C_a(r)$ takes on approximately its asymptotic value for all $r \gtrsim 7$ fm. These two properties make Eq. (34) especially useful for computing asymptotic properties of Ψ. Indeed, similar integrals tend to appear in scattering theory for exactly this reason.

Comparison of Eqs. (34) and (9) shows that, since $B_a(r \to \infty) = 0$,

$$\tan\delta_a = K_{aa} = \frac{C_a(r\to\infty)}{B_{a,\infty}}, \tag{35}$$

as discussed in many places in the literature (e.g., [34,36,48]). In fact, Eq. (35) may be improved upon significantly to yield estimates of K_{aa} that are second-order variational in approximations to Ψ [36,38,48,51]. (These improvements require considerably more computation, so I do not pursue them here.) From the discussion in Sec. II A, at resonance there is no contribution from the regular function so that $B_{a,\infty} = 0$ and K_{aa} has a pole. The residue of K_{aa} at this pole (for Ψ normalized to unity within some radius $r_{\rm norm}$ that contains the interaction region) is

$$\mathcal{R} = \frac{\hbar^2 k_a}{2\mu_a}|C_a(r\to\infty)|^2, \tag{36}$$

up to corrections of order

$$\epsilon = \frac{\hbar^2}{2\mu_a}|r_{\rm norm}R_a(r_{\rm norm})|^2\frac{d}{dE_a}\left[\frac{k_a G_{l_a}'(\eta_a, k_a r_{\rm norm})}{G_{l_a}(\eta_a, k_a r_{\rm norm})}\right], \tag{37}$$

discussed in Refs. [44,45]. It is easy to show from Eq. (8) that the residue of the S-matrix pole is twice the residue of the corresponding K-matrix pole, and thus the partial width of the resonance in channel a is given by

$$\Gamma_a = \frac{\hbar^2 k_a}{\mu_a}|C_a(r\to\infty)|^2, \tag{38}$$

again up to corrections of order ϵ. Since the integral defining C_a [Eq. (33)] is short-ranged, Eq. (38) for the partial width may be formulated as the square of a straightforward integral over all nucleon coordinates without specifying a boundary.

This result for the width is easily generalized to include bound states. These occur at negative energy, $E_a = -|E_a|$, so that $k_a = i|k_a|$ and $\eta_a = -i|\eta_a|$. Since they must be square-integrable, their overlap functions are asymptotically

$$R_a(r\to\infty) \propto O_l(\eta_a, k_a r\to\infty)/r \propto e^{ik_a r}r^{-i\eta_a - 1}. \tag{39}$$

For purely imaginary k_a, O_l is proportional to the Whittaker function, $W_{-|\eta_a|,l+\frac{1}{2}}(2|k_a|r)$. By working with analytic continuations of the linearly independent pair of functions F_l and O_l instead of F_l and G_l, an integral relation analogous to Eq. (31) may be derived. It yields a result for $R_a(r)$ that is guaranteed to have the correct form [Eq. (39)] at large r even if it is generated from an approximate Ψ that does not solve the Schrödinger equation exactly. In fact, an early use of integral relations of the form considered here was to produce overlaps with the correct asymptotic behavior from asymptotically incorrect Hartree-Fock wave functions [49,52]. They have been used more recently to compute the asymptotic normalizations α_a defined by

$$R_a(r\to\infty) = \alpha_a W_{-|\eta_a|,l_a+\frac{1}{2}}(2|k_a|r)/r \tag{40}$$

from shell-model and *ab initio* wave functions [30–33,50,53,54].

It is evident from the discussion above that a variational approximation to the wave function Ψ allows two calculations of $R_a(r)$: one from the definition in Eq. (18) and one from the integral relation of Eq. (31). If Ψ, $\psi_{a1}^{J_a}$, and $\psi_{a2}^{J_a}$ are all eigenstates of their respective Hamiltonians, both methods yield the same result. In a typical application of many-body methods, Ψ is quite accurate in the interaction region but inaccurate where the daughter nuclei are widely separated. Equation (18) yields $R_a(r)$ that is only as accurate as Ψ is at r and is not guaranteed to have the correct form at large r. If R_a is computed from Eq. (31), its value at any radius depends only on the values of Ψ within the interaction region (apart from the integration constant $B_{a,\infty}$, which is nonzero only for nonresonant open channels). At large radius the correct asymptotic shape is guaranteed. It seems likely that since Eq. (31) incorporates the Hamiltonian directly (through $U_{\rm rel}^{a,p}$) and not just through the approximate Ψ, it is also more accurate at smaller r than the directly computed $R_a(r)$ [52].

III. APPLICATION TO VARIATIONAL WAVE FUNCTIONS

In the following calculations I use variational wave functions that were computed by the VMC method. They are approximate solutions for a Hamiltonian consisting of the sum of the Argonne v_{18} (AV18) two-body [55] and Urbana IX (UIX) three-body [56] interactions, which appear both in the computation of the wave functions and in the operator $U_{\rm rel}^{a,p}$ used in the integral relation. In this section I describe enough of the structure of the VMC p-shell wave functions to discuss their asymptotic properties, I explain the implementation of the integral relation, and I finally comment on the asymptotics of the wave functions. The wave functions are described in detail in Ref. [57].

A. Variational wave functions

The VMC wave functions begin with the spin-isospin function $\Phi_\alpha(0000)_{1234}$, in which the spins and isospins of the first four particles are organized into a Slater determinant like those of a filled, α-particle-like $0s$ shell. (The zeros denote the total angular momentum J, its projection M, the total isospin T, and its projection T_z; this notation follows conventions in previous QMC work and should not be confused with the channel function Φ_a.) The addition of further particles while retaining antisymmetry requires spatial dependence in the wave function, i.e., placing particles into the p shell. This is done using orbitals $\phi_p^{LS[n]}(r_{\alpha i})$ defined in terms of the separation $r_{\alpha i}$ of particle i from the center of mass of the "α core." The orbitals are derived from Woods-Saxon potential wells and coupled to form states of definite angular momentum, parity, spatial symmetry, and isospin in an LS-coupled basis, and they fall off exponentially at large

$r_{\alpha i}$. The effects of pairwise interactions between nucleons (through the AV18 potential) are then accounted for using two-body scalar correlations $f(r_{ij})$ that mainly account for particles' avoidance of the repulsive core of the potential and are functions of the separation r_{ij} of particles i and j. It has been found advantageous to allow different scalar correlations depending on whether particles i and j are both in the s shell (f^{ss}), both in the p shell (f^{pp}), or one in each (f^{sp}). Finally, there are analogous three-body scalar correlations (f^{sss}, f^{spp}) due to both two- and three-body interactions. All of these elements (α core, LS-coupled orbitals, and scalar correlations) are antisymmetrized among particle permutations to make up the Jastrow wave function:

$$\Psi_J = \mathcal{A}\Bigg\{ \prod_{i<j<k\leqslant 4} f^{sss}_{ijk} \prod_{n\leqslant 4} \prod_{5\leqslant m<A} \prod_{m<q\leqslant A} f^{spp}_{nmq} \prod_{t<u\leqslant 4} f^{ss}(r_{tu}) \times \prod_{i\leqslant 4} \prod_{5\leqslant j\leqslant A} f^{sp}(r_{ij}) \prod_{5\leqslant k<l\leqslant A} f^{pp}(r_{kl}) \times \sum_{LS[n]} (\beta_{LS[n]} \Phi_A(LS[n]JMTT_z)_P) \Bigg\}. \tag{41}$$

The index P denotes a specific permutation of the particles into s and p shells (subsequently antisymmetrized by the operator $\mathcal{A}$) and the amplitudes $\beta_{LS[n]}$ specify the admixtures of p-shell LS states of the Young diagram $[n]$. In turn, the configuration of good L, S, $[n]$, J, M, T, and T_z is given by

$$\begin{aligned}\Phi_A(LSJM[n]TT_z)_P &= \Phi_\alpha(0000)_{1234} \prod_{5\leqslant i\leqslant A} \phi_p^{LS[n]}(r_{\alpha i}) \\ &\times \left[\left[\prod_{5\leqslant j\leqslant A} Y_{1m_j}(\hat{r}_{\alpha j}) \right]_{LM_L} \otimes \left[\prod_{5\leqslant k\leqslant A} \chi_k\left(\frac{1}{2} m_k\right) \right]_{SM_S} \right]_{JM} \\ &\times \left[\prod_{5\leqslant l\leqslant A} \nu_l\left(\frac{1}{2} t_z\right) \right]_{TT_z},\end{aligned} \tag{42}$$

where the spinors χ_i and ν_i specify the angular momentum and isospin states of particle i. Because the Hamiltonian includes operator as well as scalar terms (i.e., it acts on particle spins and isospins), there are operator correlations in addition to central correlations. These are accounted for by writing the variational trial function as

$$\Psi_T = \mathcal{S} \prod_{i<j} \left(1 + U_{ij} + \sum_{k\neq i,j} \tilde{U}^{TNI}_{ijk} \right) \Psi_J, \tag{43}$$

where U_{ij} and $\tilde{U}^{TNI}_{ijk}$ are two- and three-body operators, and $\mathcal{S}$ is a symmetrization operator, needed to preserve the antisymmetry of Ψ_J because the U_{ij} and $\tilde{U}^{TNI}_{ijk}$ do not commute among themselves. The operator correlations are of the form

$$U_{ij} = \sum_{2\leqslant q\leqslant 6} \left[\prod_{k\neq i,j} f^q_{ijk}(\mathbf{r}_{ik}, \mathbf{r}_{jk}) \right] u_q(r_{ij}) O^q_{ij}, \tag{44}$$

where f^q_{ijk} is an operator-independent three-body correlation, and the operators $\mathcal{O}^q_{ij} = \boldsymbol{\tau}_i \cdot \boldsymbol{\tau}_j$, $\boldsymbol{\sigma}_i \cdot \boldsymbol{\sigma}_j$, $\boldsymbol{\sigma}_i \cdot \boldsymbol{\sigma}_j \boldsymbol{\tau}_i \cdot \boldsymbol{\tau}_j$, S_{ij}, and $S_{ij}\boldsymbol{\tau}_i \cdot \boldsymbol{\tau}_j$ (where $\boldsymbol{\sigma}_i$ are nucleon spin operators, $\boldsymbol{\tau}_i$ are isospin operators, and S_{ij} is the tensor operator) appear in the largest operator terms in the AV18 potential. The $u_q(r_{ij})$, together with the scalar correlation $f^{ss}(r_{ij})$, solve a set of coupled Euler-Lagrange equations with coefficients that serve as variational parameters, discussed in Ref. [58]. The central correlation f^{ss} falls off exponentially to reflect the strong binding of the s-shell particles, as do the u_q functions.

The $f^{sp}(r_{ij})$ and $f^{pp}(r_{ij})$ correlations are constructed to approximate $f^{ss}(r_{ij})$ at small r_{ij} but to approach constant values at large r_{ij}. This guarantees that where particles approach each other closely the wave function is governed by the nucleon-nucleon interaction but that the correlation between widely separated particles is dominated by binding to a "mean field" accounted for in the $\phi_p^{LS[n]}$ orbitals. Thus, the asymptotic region of Ψ_T is dominated by the $\phi_p^{LS[n]}$, which have much longer tails than the f^{ss}.

All of the functions appearing so far in this section are specified as functions of variational parameters, either explicitly or in the differential equations solved to compute correlations. The optimum values of those parameters are found by searching the parameter space to minimize the energy expectation value,

$$E \leqslant \frac{\langle \Psi_T | H | \Psi_T \rangle}{\langle \Psi_T | \Psi_T \rangle}, \tag{45}$$

with both numerator and denominator computed by Monte Carlo integrals over the particle coordinates. As a final step, the Hamiltonian is diagonalized with respect to the p-shell configurations labeled by $LS[n]$ to find the coefficients $\beta_{LS[n]}$. Diagonalization both improves the variational energy of the ground state of given J^π and T and provides access to excited states.

Energies of unbound p-shell states can almost always be lowered by making their wave functions more diffuse (closer to threshold). This is also often true of bound states, where variational energies (but not GFMC energies) can lie artificially above breakup thresholds because of shortcomings of the variational ansatz. For both bound and resonance states, this problem is addressed by constraining variational parameter searches to keep charge radii close to experimentally known ground-state charge radii.

The values of the variational parameters for all states used in the present calculations were provided by Wiringa [59]. They are the results of calculations in bases of good isospin in which individual nucleons typically cannot have definite charges. For convenience in defining the integral relations for neutron or proton decays, I carry out the calculations below in a basis of good nucleon charge (essentially an m-scheme in the particle isospins) so that the emitted nucleon is definitely either a neutron or a proton. For given variational parameters, this is only a change of representation and does not alter observables. The variational minimization has in all cases been carried out for the state of lowest T_z in each isomultiplet. I compute widths of the isobaric analogs of these states by using isospin rotations of the minimized states rather than carrying out independent variational minimizations.

B. Overlap and integral-relation calculations

Calculations of explicit overlap functions $R_a(r)$ [Eq. (19)] and integral relations [Eqs. (32) and (33)] involve several common elements. While integral relations are much more time consuming because they contain the operator $U_{\rm rel}^{a,p}$, most of the computational tasks in organizing both calculations amount to constructing the channel vector $\tilde{\Phi}_{a,p}(\boldsymbol{\xi}_{a1}^{p}, \boldsymbol{\xi}_{a2}^{p}, \mathbf{r}_a)$ given by Eq. (14) and then contracting either Ψ_T or $(U_{\rm rel}^{a,p} - V_C^a)\Psi_T$ against it. For nucleon emission, I take $\psi_{a1}^{J_{a1}}$ to be the wave function of the daughter nucleus and $\psi_{a2}^{J_{a2}}$ to be the spinor of the emitted nucleon.

The integrals of Eqs. (18) and (33) are computed by Monte Carlo integration over the particle coordinates, using the same sampling algorithm that has long been used to compute the energy expectation value, Eq. (45). Sampling follows the Metropolis algorithm, using the weight function

$$W(\mathbf{R}) = \Psi_T^{\dagger}(\mathbf{R})\Psi_T(\mathbf{R}), \tag{46}$$

where $\Psi_T(\mathbf{R})$ is the variational wave function for the A-body parent nucleus at particle coordinates $\mathbf{R}$. The delta function in Eq. (18) is accounted for by sampling all particle coordinates and sorting the samples into narrow bins of specified channel radius; this builds up the entire function $R_a(r)$ from a single Monte Carlo walk. The normalization integral needed to give $\psi_{a1}^{J_{a1}}$ unit norm is computed in the same Monte Carlo walk by which the overlap or integral relation is computed.

Only relative coordinates are used in the definitions of Ψ_T and $\tilde{\Phi}_{a,p}$, so the results of the calculations are all explicitly translation invariant, and for operator

$$\mathcal{M} = \begin{cases} \delta(r_a - r)/r_a^2 & \text{(spectroscopic overlap)}, \\ F_l(\eta_a, k_a r_a)\big(U_{\rm rel}^{a,p} - V_C^a\big)/r_a & \text{(integral relation)}, \end{cases} \tag{47}$$

the quantity computed is

$$I = \frac{\langle \Phi_a | \mathcal{M} | \Psi_T \rangle}{\big\langle \psi_{a1}^{J_{a1}} \big| \psi_{a1}^{J_{a1}} \big\rangle \langle \Psi_T | \Psi_T \rangle}. \tag{48}$$

The routines used to compute the integral relations were written as modified versions of existing spectroscopic-overlap routines [60–63]. The integral-relation routines were used previously to compute bound-state ANCs [33], and only very minor modification (replacing regular Whittaker functions with regular scattering functions) was necessary for width calculations.

Finally, the operator $U_{\rm rel}^{a,p}$ must be considered. It is just the potential-energy operator of the AV18 + UIX Hamiltonian, but with the restriction that only terms involving the pth (emitted) nucleon are considered so that Eq. (24) becomes

$$U_{\rm rel}^{a,p} = \sum_{i \neq p} v_{ip} + \sum_{i<j, i\neq p, j\neq p} V_{ijp}. \tag{49}$$

Its action on Ψ_T is evaluated by calling the potential-energy routines with instructions to omit all terms purely internal to $\psi_{a1}^{J_{a1}}$ for the given permutation. It is then straightforward to contract $(U_{\rm rel}^{a,p} - V_C^a)\Psi_T$ with $[\tilde{\Phi}_{a,p}(\boldsymbol{\xi}_{a1}^{p}, \boldsymbol{\xi}_{a2}^{p}, \mathbf{r}_a)]^{\dagger}$ for a given configuration $\mathbf{R}$.

It is instructive to examine the integrand of Eq. (33) by inserting a delta function $\delta(r_a - r)/r_a^2$ into the integral. This is evaluated just like the delta function in Eq. (18), by carrying out the Monte Carlo walk for the full integral and binning the Monte Carlo samples according to the channel radius instead of summing them all together. A typical result is shown in Fig. 1, and nearly all cases that I have computed appear similar to this graph apart from an overall scaling. It is evident that the largest contribution comes from $r_a \approx 2.5$ fm. It is also evident that the form of the VMC wave function beyond ∼7 fm is irrelevant for the width, because the factor $(U_{\rm rel}^{a,p} - V_C^a)$ is zero there. This limits the integral to smaller radii and guarantees convergence of the integral regardless of what lies in the tails of the variational wave function.

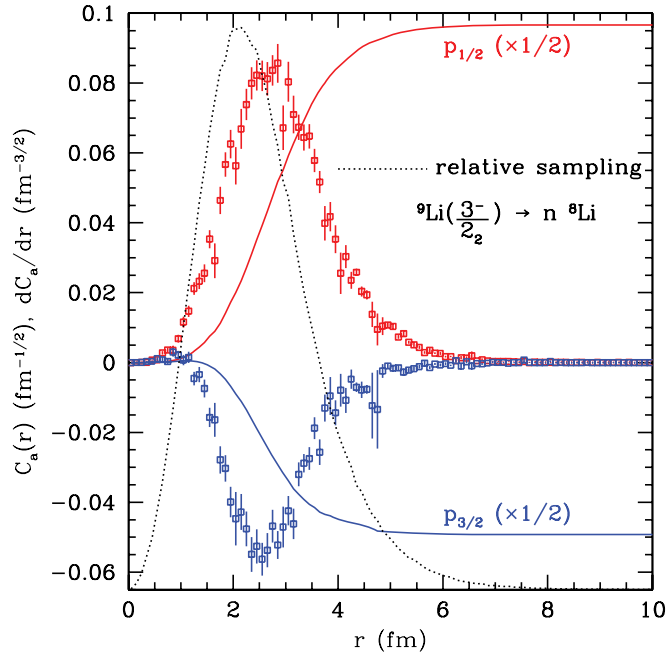

FIG. 1. (Color online) The distribution of the integrand of Eq. (33) in two j_a channels as a function of channel radius r after integrating over all other coordinates. The case shown is the ^{9}Li$(3/2_2^-)$ overlap onto ^{8}Li(g.s.) + neutron, but the shapes of the curves are similar in nearly all calculations from VMC wave functions. Discrete points show the integrand dC_a/dr. The solid curve shows its cumulative integral, $C_a(r)$, which at large radius is equal to the wave function asymptotic normalization. The integrand goes to zero at small radius because it contains the regular function $F_l(\eta_a, k_a r_a)$ and at $r_a \sim 7$ fm because $U_{\rm rel}^{a,p} - V_C^a \to 0$ there. The light dotted curve indicates the distribution of samples in the Monte Carlo integration (with zero at the bottom of the graph).

The motivation presented above for the integral relations assumes that Ψ_T, $\psi_{a1}^{J_{a1}}$, and $\psi_{a2}^{J_{a2}}$ are all energy eigenstates. To the extent that the VMC wave functions approximate these states, the integral relations approximate the overlaps and widths *of the Hamiltonian for which they are approximate solutions*. Two difficulties then present themselves in applying the integral relations to VMC wave functions: (i) comparison of the results to other calculations using the AV18 + UIX Hamiltonian is not possible because (except for ^{5}He) no such calculations have been done by other methods and (ii) comparison to experiment is complicated because experimental resonance energies are not reproduced exactly by the Hamiltonian.

The mismatch of resonance energies from experiment can be dealt with straightforwardly. The integral relations of Eqs. (32) and (33) require an assumed channel energy E_a, from which k_a and η_a are computed. Formally, E_a should be the channel energy of the AV18 + UIX Hamiltonian (known from GFMC), but the mismatch between this and the experimental E_a is often $\sim$1 MeV. Since the potential energy in the p shell is much larger (-100 to -400 MeV), the experimental E_a is close enough to the AV18 + UIX channel energy that it can plausibly be used in the integrals. (See Sec. IV A.) This choice accounts for most of the well-known strong dependence of the width on the resonance energy so that comparison with experiment is possible. It was found previously that using the experimental separation energy in integral-relation calculations of bound-state ANCs produces results in generally good agreement with experiment [33]. Similarly, the results below indicate that using the experimentally measured resonance energy as E_a allows prediction of experimental widths. I present the results of using both experimental and GFMC values of E_a in the integral relations.

More consistent calculations will require Hamiltonians that more precisely reproduce thresholds and resonance energies. Such Hamiltonians exist in the form of the Illinois three-body potentials [6,64], but they have not yet been incorporated into the VMC code used here, and $U_{\rm rel}^{a,p}$ for these interactions requires considerably more computation than for the UIX interaction.

C. The asymptotic forms of VMC wave functions

Consider configurations in which particle A (before antisymmetrization) is far from the first $A-1$ particles. Because f^{pp} and f^{sp} approach constants and f^{ss} decays rapidly at large r_{ij}, the shape of Ψ_T in this part of the wave function is dominated by the shapes of the single-particle functions $\phi_p^{LS[n]}$. This might be expected to give

$$R_a(r \to \infty) \approx \sum_{LS[n]} \gamma_{LS[n]} \phi_n^{LS[n]}(\omega_{LS[n]} r) \qquad (50)$$

for some amplitudes $\gamma_{LS[n]}$ and Jacobian-like factors $\omega_{LS[n]}$ that emerge from the correlations of Eqs. (41)–(43) when the overlap integral is computed. The factors $\omega_{LS[n]}$ account for the distinction between the channel radius r and the distance $r_{\alpha i}$ of a p-shell particle from the center of mass of the s-shell core; these only coincide when $A = 5$ and otherwise differ by the mean difference between nucleon-core and nucleon-daughter distances.

In general, the $\phi_p^{LS[n]}$ that emerge from the variational procedure do not yield the correct long-range asymptotic shapes for the overlaps R_a. This is most readily seen for open channels, where solutions that should oscillate at large channel radius instead fall off with an assumed exponential dependence. In closed channels, the condition of square integrability gives zero for the analog of $B_{a,\infty}$ in Eqs. (31) and (34), so that Eq. (40) holds for the true wave function. Because no single $LS[n]$ term typically dominates a given $R_a(r)$, it is in general difficult to construct $\phi_p^{LS[n]}$ to satisfy Eq. (40) for all possible channels at once. This difficulty is compounded by the problem that the energy expectation value driving the variational minimization receives very little contribution from the wave function tails, so the variational principle does not constrain the low-probability tails of the wave function very strongly. The application of the integral approach to bound-state ANCs in Ref. [33] avoided these difficulties and effectively matched the correct asymptotic form onto the better-computed interior of the wave function.

Pseudobound VMC wave functions approximate resonance states with square-integrable wave functions, in which the f^{ss} and $\phi_p^{LS[n]}$ functions cut off the wave function tails exponentially. This exponential cutoff can be understood at "medium" range (4–8 fm) as forcing a resonance form on the wave function and beyond this range as providing a regularization to normalize the unbound state despite its formally nonzero amplitude at large radius. Such a regularization is important for quantities such as electromagnetic transition strengths (e.g., [65,66]) and for the approximate relation between the asymptotic normalization and the partial width given in Eq. (38) [45]. As long as the resonance wave function is computed reasonably accurately within the region where the integral of Eq. (33) is nonzero, and it is normalized to unity over the region where Ψ_T is larger in amplitude than in the asymptotic region, the integral approximates the asymptotic normalization of G_l and thus the partial width. The cutoff of Ψ_T at large nucleon separation is illustrated with overlap functions in Fig. 2.

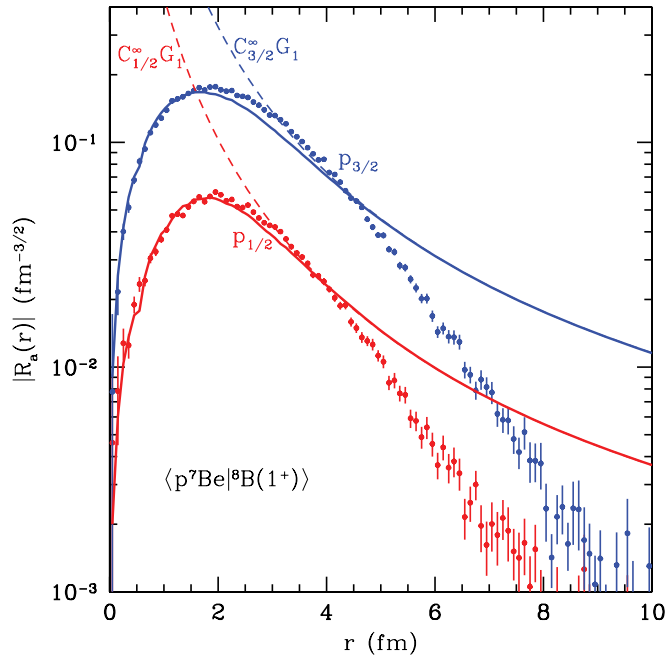

FIG. 2. (Color online) Overlaps $R_a(r)$ of the unbound $J^\pi = 1^+$ state of ^{8}B onto ^{7}Be + proton, computed directly from Eq. (18) (discrete points with Monte Carlo error bars) and from the integral relation of Eq. (31) (solid curves). At large radius, the directly computed overlap falls off exponentially because the $\phi_p^{LS[n]}$ in the VMC wave function fall off exponentially. However, the integral-relation overlap (with $B_{a,\infty} = 0$) gives the exact proportionality to G_l expected at resonance. The absolute normalization $C_{ja}^{\infty} \equiv C_a(r \to \infty)$ multiplying G_l gives the partial width of ^{8}B(1^+) in each ^{7}Be + p channel; the normalized asymptotic is shown as a dashed curve for each channel and manifestly merges with the full overlap at $\gtrsim$4 fm.

TABLE I. The results of integral-relation calculations of widths. Results are shown from calculations in which the channel energy was assumed equal to its experimental value ("From expt. energy") and to the AV18 + UIX channel energy known from GFMC ("From AV18 + UIX energy"). Error estimates are quadrature sums of Monte Carlo sampling errors and uncertainties from the input energies. Where no experimental energy is available, the results in the "Experiment" columns were computed using the GFMC energy with the AV18 + IL7 Hamiltonian, and they are indicated by square brackets. The column "Matches $\pi/2$?" indicates whether the overlap function appears consistent with a resonance state, as discussed in Sec. IV A. See Sec. IV A and Eq. (52) for the definition of ζ. Energies are relative to the decay threshold in the center-of-mass frame. Experimental energies are taken from data compilations [67,68] unless otherwise noted.

State	Daughter	Experiment		From expt. energy	From AV18 + UIX energy		Matches	ζ
		E (MeV)	Γ (MeV)	$\Gamma_{\rm VMC}$ (MeV)	$E_{\rm UIX}$ (MeV)	$\Gamma_{\rm VMC}$ (MeV)	$\pi/2$?	
^{5}He($3/2^-$)	^{4}He(0^+)	0.798	0.648 [67]	0.307(5)	1.39	0.684(11)	no	0.460
^{5}He($1/2^-$)	^{4}He(0^+)	2.07	5.57 [67]	0.582(13)	2.4	0.711(15)	no	0.429
^{7}He($3/2^-$)	^{6}He(0^+)	0.445(3)	0.122(13)[a]	0.114(12)	1.68(13)	0.77(10)	yes	0.092
^{7}He($1/2^-$)	^{6}He(0^+)	3.05(10)[b]	–	1.98(12)	2.83(13)	1.80(12)	no	0.21
^{7}He($1/2^-$)	^{6}He(2^+)	1.25(10)[b]	–	0.42(6)	0.89(13)	0.26(5)	yes	0.067
^{7}He($1/2^-$)	sum		2.0(1.0)[c]	2.40(12)[d]	2.83(13)	2.22(11)[d]		
^{7}He($5/2^-$)	^{6}He(2^+)	1.55(3)[b]	1.99(17) [67]	1.29(12)[d]	1.87(13)	1.7(2)[d]	no	0.165
^{7}Li($5/2^-_2$)	^{6}Li(1^+)	0.204	0.065(3) [67]	0.0483(17)[d]	1.57(17)	0.92(13)[d]	yes	0.055
^{7}Be($5/2^-_2$)	^{6}Li(1^+)	1.60(6)	0.19(5) [69]	0.43(4)[d]	2.65(17)	1.11(14)[d]	yes	0.055
^{8}Li(3^+)	^{7}Li($3/2^-$)	0.223(3)	0.032(3) [70]	0.0344(18)	2.10(18)	0.88(11)	yes	0.007
^{8}Li(0^+)	^{7}Li($3/2^-$)	[0.97(13)]	–	[0.37(7)]	0.67(17)	0.24(8)	no	0.005
^{8}Li(0^+)	^{7}Li($1/2^-$)	[0.847(14)]	–	[0.81(2)]	0.78(17)	0.7(2)	no	0.004
^{8}Li(2^+_2)	^{7}Li($3/2^-$)	[2.18(16)]	–	[1.00(11)]	–	–	yes	0.004
^{8}Li(2^+_2)	^{7}Li($1/2^-$)	[2.06(19)]	–	[0.105(14)]	–	–	yes	0.010
^{8}Be(1^+) $T=1$[e]	^{7}Li($3/2^-$)	0.385(1)	–	0.0089(3)	1.26(19)	0.17(5)	yes	0.003
^{8}Be(1^+) $T=0$[e]	^{7}Li($3/2^-$)	0.895(5)	–	0.152(4)	0.51(21)	$0.04^{+0.05}_{-0.03}$	yes	0.003
^{8}Be(1^+) sum[e]	^{7}Li($3/2^-$)		0.149(6) [68]	0.161(4)		0.21(5)	yes	
^{8}Be(3^+) $T=1$[e]	^{7}Li($3/2^-$)	1.81(3)	–	0.166(9)	3.68(18)	0.60(7)	yes	0.007
^{8}Be(3^+) $T=0$[e]	^{7}Li($3/2^-$)	1.98(1)	–	0.314(14)	2.3(2)	0.43(7)	yes	0.003
^{8}Be(3^+) $T=1$[e]	^{7}Be($3/2^-$)	0.17(3)	–	0.012(3)	2.14(18)	0.45(5)	yes	0.007
^{8}Be(3^+) $T=0$[e]	^{7}Be($3/2^-$)	0.335(10)	–	0.050(3)	0.8(2)	0.18(6)	yes	0.004
^{8}Be(3^+) sum[e]	sum		0.50(3) [68]	0.542(17)		1.66(13)	yes	
^{8}B(1^+)	^{7}Be($3/2^-$)	0.632(3)	–	0.0382(15)	1.3(3)	0.26(13)	yes	0.001
^{8}B(1^+)	^{7}Be($1/2^-$)	0.203(3)	–	0.00105(8)	1.4(2)	0.5(2)	yes	0.003
^{8}B(1^+)	sum		0.0357(6) [68]	0.0394(15)		0.8(2)	yes	
^{8}B(3^+)	^{7}Be($3/2^-$)	2.18(2)	0.39(4)[f]	0.38(2)[d]	3.7(2)	1.08(11)[d]	yes	0.007
^{8}B(0^+)	^{7}Be($3/2^-$)	[2.55(13)]	–	[0.65(7)]	2.17(17)	0.47(8)	no	0.005
^{8}B(0^+)	^{7}Be($1/2^-$)	[2.44(14)]	–	[1.46(18)]	2.30(13)	1.3(2)	no	0.004
^{8}B(2^+_2)	^{7}Be($3/2^-$)	2.41(2) [71]	0.12(4) [71]	0.51(2)	–	–	yes	0.004
^{8}B(2^+_2)	^{7}Be($1/2^-$)	1.98(2) [71]	0.24(11) [71]	0.039(2)	–	–	yes	0.010
^{9}Li($5/2^-$)[g]	^{8}Li(2^+)	0.232(15)	0.10(3) [63]	0.145(14)	0.98(44)	1.2(8)	yes	0.003
^{9}Li($7/2^-$)[g]	^{8}Li(2^+)	2.366(15)	–	0.0012(5)	3.6(3)	0.0031(13)	no	0.045
^{9}Li($7/2^-$)[g]	^{8}Li(3^+)	0.111(15)	–	0.043(8)	0.23(35)	<0.50	yes	0.006
^{9}Li($7/2^-$)[g]	sum		0.04(2) [63]	0.044(8)[d]		<0.50[d]		
^{9}Li($3/2^-_2$)[g]	^{8}Li(2^+)	1.32(6)	–	0.52(4)	1.5(4)	0.6(2)	no	0.014
^{9}Li($3/2^-_2$)[g]	^{8}Li(1^+)	0.34(6)	–	0.17(5)	0.5(4)	<0.7	yes	0.006
^{9}Li($3/2^-_2$)[g]	sum		0.6(1) [63]	0.69(6)[d]		0.9(4)[d]		
^{9}Be($1/2^-$)	^{8}Be(0^+)	1.11(12)	0.86(9)[h] [72]	0.80(12)[d]	4.4(6)	4.8(8)[d]	yes	0.0005

TABLE I. *(Continued.)*

State	Daughter	Experiment		From expt. energy	From AV18 + UIX energy		Matches	ζ
		E (MeV)	Γ (MeV)	$\Gamma_{\rm VMC}$ (MeV)	$E_{\rm UIX}$ (MeV)	$\Gamma_{\rm VMC}$ (MeV)	$\pi/2$?	
^{9}Be($7/2^-$)	^{8}Be(0^+)	4.72(6)	–	0.0082(3)	–	–	yes	0.005
^{9}Be($7/2^-$)	^{8}Be(2^+)	1.69(6)	–	0.40(3)	–	–	yes	0.003
^{9}Be($7/2^-$)	sum		1.2(2) [73]	0.41(3)[d]	–	–	yes	
^{9}B($3/2^-$)	^{8}Be(0^+)	0.185(1) [74]	0.00054(21) [75]	0.00058(2)[d]	1.9(3)	0.9(3)[d]	yes	0.0003
^{9}B($7/2^-$)	^{8}Be(2^+)	4.13(6)	2.0(2) [68]	0.82(4)[d]	–	–	yes	0.003
^{9}C($1/2^-$)	^{8}B(2^+)	0.918(11)	0.10(2) [76]	0.102(5)	1.5(3)	0.43(26)	yes	0.006

[a]I have computed an "observed" width of 112 ± 15 keV from the R-matrix formal width of Ref. [77] and averaged it with the 160 ± 30 keV FWHM of Ref. [78].
[b]From [79], based on ground-state energy from [67].
[c]This is reported in Ref. [62] as "≈2 MeV" with no quantitative error; a 1-MeV error is used in Figs. 3, 8, and 9 and in quoted statistics.
[d]Open channels other than one-nucleon emission were neglected in the calculation (α or nonsequential).
[e]See Sec. IV B for discussion of the effects of isospin mixing in the observed 1^+ and 3^+ states of ^{8}Be.
[f]Originally reported in Ref. [80], this number is construed in later work as the FWHM in the laboratory frame; since the center-of-mass excitation energy is reported in the same sentence, it appears to me to be a center-of-mass width. Its error has apparently been mistranscribed in later references, independent of this ambiguity.
[g]Spin-parity assignments for ^{9}Li follow Ref. [63]; see Sec. IV C3.
[h]The data compilations [68] average the reported R-matrix formal width corresponding to this number with the much less certain Breit-Wigner width of Ref. [81].

IV. RESULTS

I now apply the integral relation of Eqs. (38) and (33) to compute widths of several unbound energy levels in nuclei of mass numbers $5 \leqslant A \leqslant 9$, from VMC wave functions. I mostly choose energy levels that empirically have small width (under 1 MeV) and are dominated by nucleon emission. The integral relation is valid for decay channels in which all three wave functions (one parent and two daughters) are known, but I limit this first examination to nucleon-emission channels, where one "daughter nucleus" is a neutron or proton. I concentrate on two-body final states, but I also model some three-body decays as sequential processes, e.g., the ^{9}B ground state decaying to a proton and the unbound ground state of ^{8}Be. The subsequent decay of ^{8}Be to two α particles can be neglected because of its small width. (In principle the widths of unbound daughter states should be integrated over, but I find that in all cases considered this correction is much smaller than either the experimental errors or the widths of omitted decay channels.)

The results of the width calculations are shown in Table I. Each calculation was carried out twice: once assuming the channel energy E_a from the AV18 + UIX Hamiltonian (known from GFMC calculations) and once using the experimentally known resonance energy. (For the second $J^\pi = 2^+$ states in ^{8}B and ^{8}Li and the $J^\pi = 7/2^-$ states in ^{9}Be and ^{9}B, AV18 + UIX energies have never been computed with GFMC.) Where the experimental channel energy is unknown or uncertain, I have used instead the GFMC energy for the AV18 + IL7 Hamiltonian, which gives a better overall fit to experimental energies than AV18 + UIX.

I have taken the experimental energies and widths in Table I mainly from data compilations [67,68]. Nearly all of the widths in the compilations are "observed" widths, which coincide with the full width at half maximum (FWHM) of cross section peaks and are proportional to the sum of the K-matrix pole residues. The integral-relation widths should correspond to these quantities. In two cases [^{7}Li($5/2^-_2$) and ^{9}Be($1/2^-$)], examination of the source literature indicated that the available experimental widths are "formal" widths of the R-matrix formalism. I have converted the experimental widths listed for those states to "observed" widths by the usual relation

$$\Gamma_{\rm obs} = \frac{2\sum_a \gamma_a^2 P_{l_a}(k_a b)}{1 + \sum_a \gamma_a^2 S'_{l_a}(E_a)}, \tag{51}$$

where b (taken to be 4 fm) is a matching radius, $S_l(E)$ is the shift function of R-matrix theory [40], prime denotes its derivative, and γ_a^2 is defined by the formal width $\Gamma_a \equiv 2\gamma_a^2 P_{l_a}(k_a b)$ and the penetrability function $P_{l_a}(k_a r)$. (See the section "Definitions of resonance parameters" in Ref. [67].) The sources of the experimental widths are indicated in Table I.

The widths presented in the table are sums over all p- and f-wave decay channels. The predicted f-wave contributions are less than 1% of the total in all cases except for the decay of ^{9}Li($7/2^-$) to ^{8}Li(2^+), where it is computed to be 23% of the total. The p-wave decays are in most cases sums of $p_{1/2}$ and $p_{3/2}$ contributions. The decompositions into $p_{1/2}$ and $p_{3/2}$ (or into a channel-spin coupling scheme) are available on request from the author.

The table only includes cases for which established experimental or GFMC energies are available. I have also computed widths of several states of ^{9}He with varying assumptions about

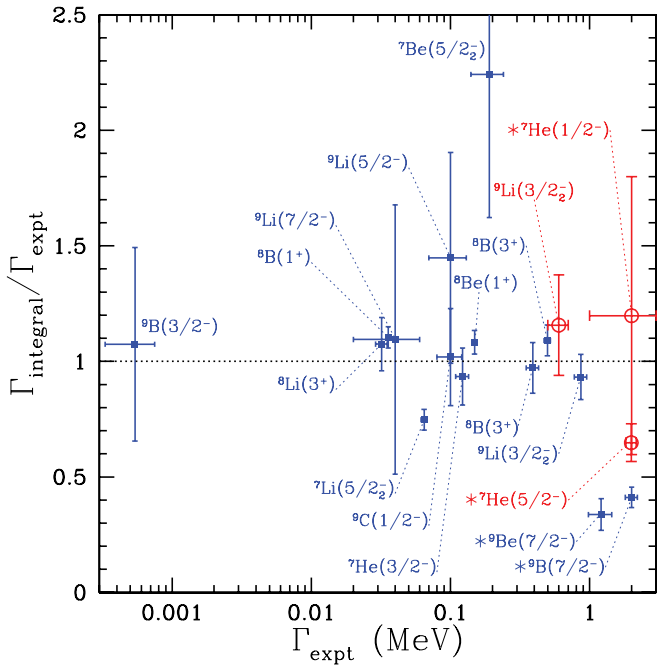

FIG. 3. (Color online) The results of Table I for those cases included in the averages. The vertical axis shows the ratio $\Gamma_{\rm integral}/\Gamma_{\rm expt}$ of the integral-relation width to the measured width, and the horizontal axis shows the measured width $\Gamma_{\rm expt}$. The horizontal dotted line shows $\Gamma_{\rm integral} = \Gamma_{\rm expt}$ as a guide to the eye. The errors shown are dominated by those on the experimental widths. Experimental errors have been added in quadrature to smaller Monte Carlo statistical errors and errors propagated from the energy used in computing $\Gamma_{\rm integral}$. States for which important α or three-body decays have been neglected are indicated with asterisks next to the state labels, and large (red) circles indicate overlaps that seem inconsistent with a $\pi/2$ phase shift. The outlying $5/2_2^-$ states of ^{7}Be and ^{7}Li are complicated by the need to include the small α-decay channel in multichannel R-matrix fits when extracting widths from data; this introduces a considerable spread in reported nucleon widths [67].

resonance energies as described below, but I have not included these numbers in Table I.

The computed widths of those states and channels for which experimental data are available are shown graphically in Fig. 3. Only for those states where partial widths are available from experiment do I show partial widths in the graphs; otherwise total widths are shown. Figure 3 demonstrates the wide dynamic range of the integral method, extending from 0.0005 to roughly 1 MeV. With the exception only of the very broad ^{5}He states, which present problems discussed below, all computed widths are within a factor of 3 of experiment and within a factor of 2 if states with uncomputed α and direct three-body width are omitted. The error-weighted mean ratio $\langle\Gamma_{\rm integral}/\Gamma_{\rm expt}\rangle$ of the integral-method width to the experimental width is 0.82 ± 0.29, and the χ^2 statistic for the difference between computed and experimental widths is 5.9 per degree of freedom (for 19 total states after omitting ^{5}He). Restricting consideration to those states with no omitted channels gives $\langle\Gamma_{\rm integral}/\Gamma_{\rm expt}\rangle = 1.09 \pm 0.04$ and $\chi^2_\nu = 1.5$ with $\nu = 9$. The errors used to compute these statistics are mainly in the measured width $\Gamma_{\rm expt}$.

Apart from the resonance energies, the main sources of uncertainty in the theoretical calculation are in the accuracy of the variational wave function and of the potential. Because it is unclear how to estimate these errors, the theoretical errors reported in Table I are the quadrature sums of Monte Carlo sampling errors with errors propagated from the input resonance energies. Errors propagated from experimental energies are typically small compared with the other errors. However, each GFMC channel energy is the difference of a resonance energy and a threshold energy from separate calculations. The error on this difference is often large compared with the channel energy, and this propagates to a large error on the predicted width.

A. Correspondence of computed states to resonance states

The results presented in Table I and Fig. 3 vary in the degree to which they match the experimental widths. Some, such as the first 3^+ state of ^{8}Li, are close matches. Others, such as the two low-lying states of ^{5}He, are very far from agreement with experiment. The ^{5}He cases are particularly interesting, because they are the only ones for which the correct widths for the AV18 + UIX Hamiltonian are known from explicit scattering calculations [11]. The known AV18 + UIX widths are 1.5 MeV for the $3/2^-$ state and 5.0 MeV for the $1/2^-$ state, while applying the integral relation to the pseudobound VMC wave functions gives 0.68 and 0.71 MeV, respectively. The $1/2^-$ state lies above the centrifugal barrier and is so broad that its phase shift does not pass through $\pi/2$, so it is unsurprising that the integral method fails for this case. The $3/2^-$ state does not present these difficulties, so its difference from both experiment and theory is clearly not a shortcoming of the potential but rather of the computational methods.

There are several reasons why the application of the integral relation to a pseudobound variational wave function could fail to yield the correct width for the potential. I begin by noting that, for the states examined, the function $F_{l_a}(\eta_a, k_a r_a)$ typically does not deviate far from its leading-order dependence on $k_a r_a$ over the range of r_a where $U^{a,p}_{\rm rel} - V^a_C$ differs significantly from zero. The main effect of changing the assumed resonance energy is therefore to change the overall scale of the integrand in Eq. (33) without changing its shape much. Thus, simply using the experimental channel energy in the integral relation should correct rather accurately for the mismatch between experimental and theoretical channel energies without introducing significant distortions in the integrand.

It is possible that the variational minimization with constrained charge radius fails to produce good approximations to some resonance states. It could happen that the variational ansatz is a poor match to a particular resonant wave function or that the VMC wave function, being only approximate, contains "contamination" from nonresonant continuum states. Contamination more energetic than the desired state is precisely what the GFMC method is intended to remove, and much of the success of the QMC methods lies in the exclusion of low-energy excitations from the variational wave function. Any off-resonance contamination produces contributions to the integral relation that do not correspond to the pole residue. The danger of contamination would seem to grow with the

resonance width, because a less-peaked density of states implies a wider range of states that are similar to the resonance and difficult to eliminate by variational minimization. The presence of nearby resonances in the same channel may compound this problem by contributing contamination with rather different structure from the resonant wave function being sought.

Yet another kind of difficulty lies in the normalization of the wave function. The relationship between the width and the asymptotic normalization of standing-wave states found in Refs. [42,44,45] depends on the wave function being normalized in a finite volume and its amplitude being small at the boundary of that finite volume as expressed in Eq. (37). I have assumed that the normalization volume is effectively defined by the exponential fall-off of the f^{ss} and $\phi_p^{LS[n]}$ correlations in the tails of the variational wave function. If either the true or the computed wave function fails to fall off rapidly enough, the normalization is problematic in ways that can be viewed either as the lack of an effective cutoff or as neglect of a large surface-amplitude correction.

The normalization problem is perhaps the most straightforward to examine. The final column of Table I displays a parameter

$$\zeta = \left(\frac{8 \text{ fm } \times \ R_a(8 \text{ fm})}{r_{\max} R_a(r_{\max})} \right)^2, \tag{52}$$

where $r_{\max}$ is the location of the maximum $|R_a(r)|$, and $R_a(r)$ is computed directly from Eq. (18). This ratio measures the amplitude of the variational wave function just outside the interaction region relative to that in the interior (accounting for the r^2 dependence of the volume of a spherical shell). We may expect to encounter difficulties when $\zeta \gtrsim 0.1$, and this occurs for four states: the two ^{5}He states and the $1/2^-$ and $5/2^-$ states of ^{7}He. The relevance of ζ may also be viewed in light of Eq. (37). If I adopt 8 fm as the effective boundary of the normalization volume and assume (cf. Fig. 5 below) that typically $R_a(8 \text{ fm}) \sim 0.02 \text{ fm}^{-3/2}$, then Eq. (37) gives $\epsilon < 0.2$ for all but a very few of the widths computed here. Much larger values of ϵ occur for ^{5}He$(1/2^-)$, ^{7}He$(1/2^-)$, and minor decay channels of a few other states.

The overlap functions may also be tested for consistency with expectations for a resonance. The integral relation for the width is the $r \to \infty$ limit of R_a as computed from Eq. (31). Given a wave function and $B_{a,\infty}$, it is possible to compute the overlap function at all radii using Eq. (31), and the result is likely to be more accurate than that from direct calculation of R_a.

Determining $B_{a,\infty}$ from a variational wave function is a tractable problem [36,38], but I do not pursue it here. Since I have tacitly assumed in computing widths that $B_{a,\infty} = 0$ as required for a resonance state [cf. Eq. (35)], I can compute the full overlap function from the integral relation [Eq. (31)] with $B_{a,\infty} = 0$ and check that it matches the overlap function computed directly from Eq. (18). If the two overlaps are in rough agreement in the interaction region, then the VMC wave function is consistent with a resonance wave function and may validly be used to compute a width.

As a test of the approach, I apply it to bound states, since their integration constant corresponding to $B_{a,\infty}$ is zero by definition. Results are shown for several states in Fig. 4, and I have computed them for all of the channels considered in Ref. [33]. The agreement between the two calculations, especially for s-shell nuclei where the VMC method is more accurate, is excellent. The deviations of the integral-relation overlap from the direct overlap are likely to be improvements: the integral relation contains more information about the potential than does the VMC wave function by itself, and it guarantees the correct $r \to \infty$ asymptotics. For some nuclei with $A = 3$, 4, and 7, GFMC calculations of overlaps exist (albeit for the AV18 + IL7 Hamiltonian, not AV18 + UIX) [60]. The results of the GFMC calculations (dashed curves of Fig. 4) are not severely different from those of applying the integral method to VMC wave functions, and they deviate from the VMC direct overlaps by similar amounts. This experience with bound states indicates that overlaps computed from integral relations are at least as accurate as directly computed overlaps of VMC wave functions and are not in conflict with GFMC results. They may therefore be very useful for calculations of spectroscopic factors and transfer and knockout cross sections.

Overlap functions are shown for ^{8}B(1^+) in Fig. 2 and for several other resonance states in Fig. 5. These were computed both directly and by integral relations with $B_{a,\infty} = 0$. In all cases, the integral relation replaces the artificial exponential fall-off of the VMC wave function with the oscillatory behavior of G_{l_a}. Based on experience with bound states, the two overlaps should agree at $r \lesssim 4$ fm. In some cases [e.g., ^{9}C$(1/2^-)$] the match there is quite good, while in others [e.g., $\langle n\, ^6\text{He}|^7\text{He}(1/2^-)\rangle$] overlaps from the two methods seem to have little to do with each other. I conclude that when results of the two methods are qualitatively very different inside 4 fm, there is an inconsistency with the assumption of $\pi/2$ phase shift so that the pseudobound VMC wave function may not allow accurate width calculations. The penultimate column of Table I indicates for each width a qualitative judgment of whether the two methods of computing overlaps agree, and cases where they do not are indicated in Fig. 3 by large (red) circles. Examination of the table reveals that with the exception of the 0^+ state in ^{8}B, failures of the "$\pi/2$ assumption" occur only in a few neutron emission channels and in no proton emission channels. Considering only states consistent with $\delta_l = \pi/2$, I find $\langle \Gamma_{\text{integral}}/\Gamma_{\text{expt}} \rangle = 0.83 \pm 0.30$ and $\chi^2_\nu = 6.3$, this time for $\nu = 15$ instead of 18. Further restriction to states in which all decay channels are computed gives $\langle \Gamma_{\text{integral}}/\Gamma_{\text{expt}} \rangle = 1.08 \pm 0.04$ and $\chi^2_\nu = 1.6$ for eight degrees of freedom. These are essentially the same results as for the entire data set. It appears that the best predictor of whether a calculated width will match experiment is simply whether the calculation includes all channels contributing to the measured width.

B. Isospin mixing in ^{8}Be

A difficulty presents itself in considering the pair of $J^\pi = 3^+$ states of ^{8}Be at ∼19 MeV and the pair of 1^+ states at

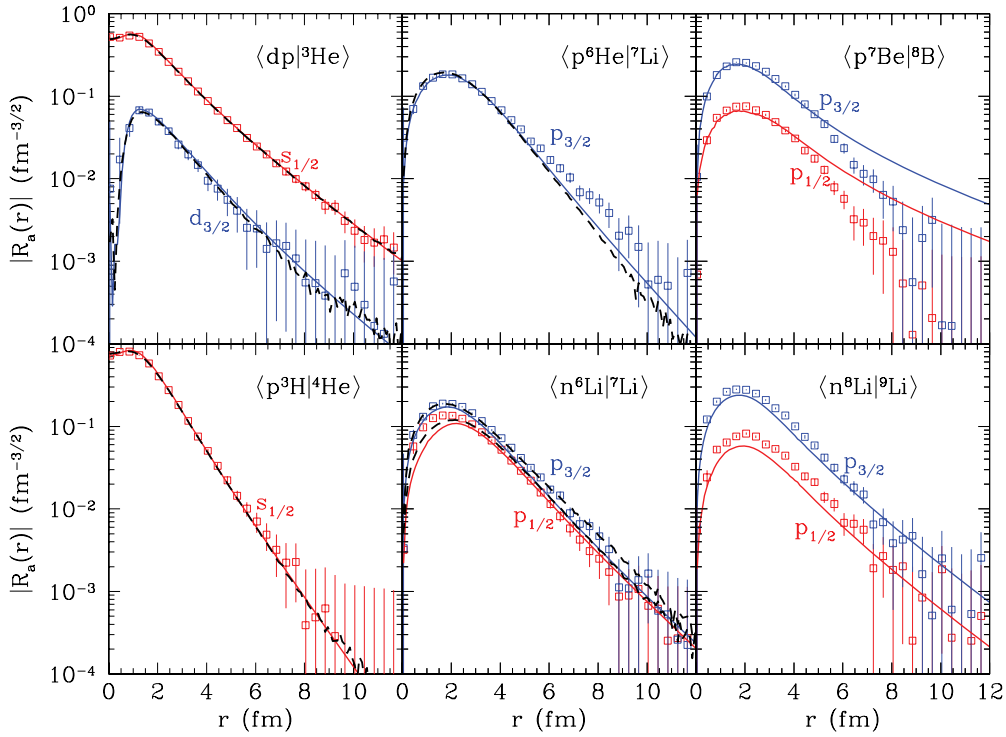

FIG. 4. (Color online) Overlap functions for several bound states, computed from the bound-state analog of the integral relation in Eq. (31) (solid curves) and from the definition in Eq. (18) (squares with Monte Carlo error bars.) The l_a and j_a quantum numbers of the "virtually emitted" nucleon are indicated by labels near the appropriate curves (and distinguished by color). Where they exist, overlaps computed directly from GFMC wave functions [60] are shown as (black) dashed curves.

∼18 MeV. Each of these doublets consists of one $T = 0$ and one $T = 1$ state that have mixed, with the lower state of each pair predominantly $T = 1$. The VMC wave functions have definite isospin, so incorporating the mixing into calculations of their widths presents ambiguities. Simply ignoring the mixing and assigning the $T = 1$ widths to the lower states and $T = 0$ widths to the higher states does not work. For example, in the 3^+ doublet, the lower state has measured width 270 ± 20 keV and the upper has 227 ± 20 keV; the unmixed widths from the integral method are 177 and 364 keV, respectively.

There exist preliminary GFMC calculations of the mixing matrix element of the Hamiltonian for each of these doublets [59], and this matrix element can be combined with the splitting of the doublet to determine its mixing angle (e.g., [82]). The splittings of the doublets are small enough that they are not resolved by the existing GFMC calculations, so the experimental splittings must be used to compute mixing angles. Since the recommended [68] 165-keV splitting of the 3^+ doublet is less than twice the GFMC mixing energy, these two numbers cannot be combined to yield a real mixing angle. (Adopting a splitting of 310 keV [83] produces good agreement with the experimental widths.) In the 1^+ doublet, combining the GFMC mixing matrix element with the experimental splitting produces a poor match to the data (widths of 14.2 and 105 keV versus 10.7 ± 0.5 and 138 ± 6 keV from experiment).

For each doublet, a mixing angle can be computed by χ^2 minimization of the difference between theoretical and experimental widths. This produces good agreement with the measured widths, which was not guaranteed. The resulting mixing angle for the 3^+ doublet has $\sin\theta_{\rm mix} = 0.28$, which is small relative to literature values [83]. The mixing angle from minimizing χ^2 for the 1^+ doublet has $\sin\theta_{\rm mix} = 0.068$, which is much smaller than both the value of 0.20 from the GFMC mixing energy and the literature value of 0.21 [84].

Thus, attempts to compute separate widths for the upper and lower states in each doublet run aground on the problem of finding mixing angles consistent with all available information. For each doublet, the quantity most independent of the mixing angle is the sum of the two widths. The sum is less sensitive to $\theta_{\rm mix}$ than are the underlying pole residues, but it is not quite independent of $\theta_{\rm mix}$ because the doublet states are not degenerate. It is the sum for each doublet that is shown in Table I and Fig. 3, with the $T = 1$ width computed in each case using the lower energy and the $T = 0$ width the higher. These sums are in good agreement with experiment.

C. Applications to recent measurements

An important use of theoretical estimates of widths is in the identification of observed states. Most of the states considered here ($A \leqslant 9$, $\Gamma \lesssim 1$ MeV, dominated by nucleon decays) were found experimentally, and their spins and parities identified, long ago. Some exceptions are the first 0^+ and second 2^+ states of ^{8}B and the entire low-lying spectra of ^{9}He and ^{9}Li. Here I attempt to shed light on these systems by calculating widths from VMC wave functions.

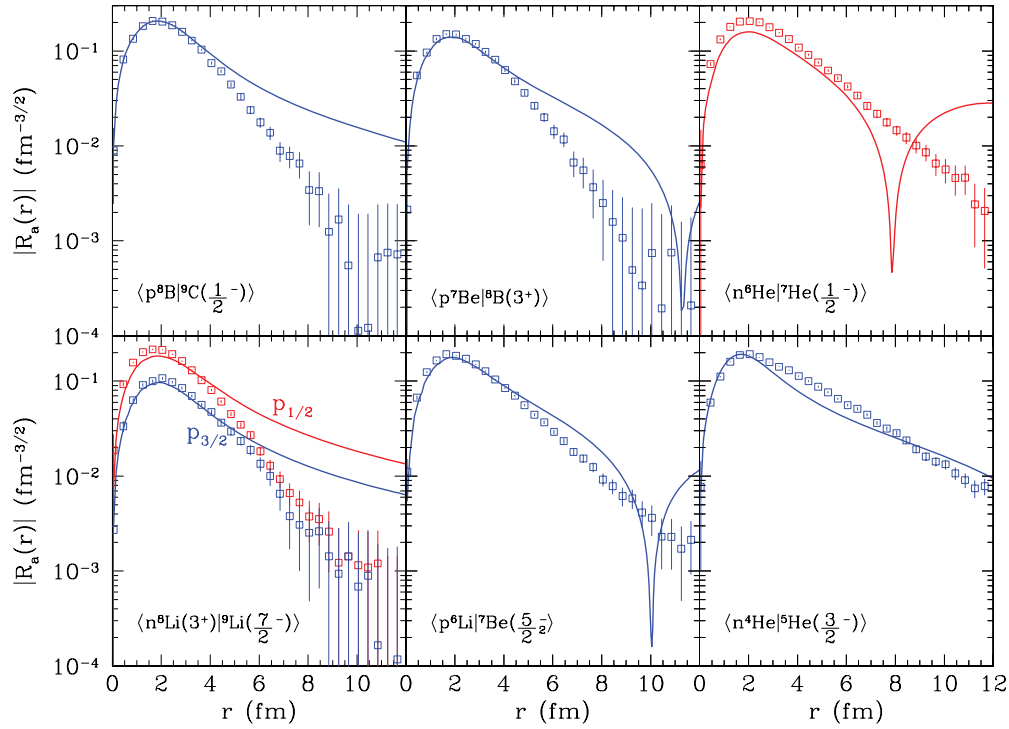

FIG. 5. (Color online) Overlap functions of several resonance states, computed directly from the definition [Eq. (18); points with Monte Carlo errors] and from the integral relation of Eq. (31) with $B_{a,\infty} = 0$ (or $\delta_{l_a} = \pi/2$; solid curves). Where more than one angular momentum channel is available, the channels are labeled. The four cases on the left show good agreement between the two methods at small separation ($r \lesssim 4$ fm), and the corresponding widths agree with experiment. The two states on the right are inconsistent with the $\delta_{l_a} = \pi/2$ assumption since the two types of overlap calculations disagree at $r < 4$ fm. Computed widths of these two states also disagree with experiment.

1. ^{8}B

Several theoretical models predict low-lying states of ^{8}B that have not been observed, as discussed in Ref. [71]. It is possible that the states are simply too broad to be seen easily in experiments, and evidence was recently found for a 0^+ state at 1.9 MeV above the ^{8}B ground state [71]. An R-matrix fit to both elastic and inelastic scattering of ^{7}Be on protons indicated a 0^+ state with partial width 0.28 ± 0.14 MeV for decay to the ^{7}Be ground state and 0.33 ± 0.18 MeV to the first excited state. Since these widths are within 2σ of zero, I have not shown them in Table I. This state has some support from the calculation of Ref. [14], where it was found in computed phase shifts at the same energy using the merged no-core shell model and resonating group method. That calculation also indicates reason for caution in applying the integral relation: the phase shift does not approach $\pi/2$, and indeed the VMC 0^+ state fails the $\pi/2$ consistency test discussed above.

I show in Table I the predicted partial widths of the 0^+ state at its energies for the AV18 + UIX and AV18 + IL7 Hamiltonians. Figure 6 shows the dependence of this prediction on the assumed resonance energy. The claimed experimental widths are consistent with my results, though inconsistency of the overlaps with $\pi/2$ phase shift makes the significance of this consistency doubtful. I also include in Table I the AV18 + IL7 energies and VMC-computed partial widths of the unobserved isobaric-analog state in ^{8}Li. The ^{8}Li and ^{7}Li VMC wave functions are explicitly isospin rotations of the ^{8}B and ^{7}Be wave functions, and the ^{8}Li(0^+) decays also fail the $\pi/2$ condition on the overlaps.

The authors of Ref. [71] also find a 2^+ state at 2.55 MeV excitation. Because this result has not been confirmed, I omit this state from goodness-of-fit statistics, but I have computed its partial widths to the ^{7}Be ground and first-excited states and included the results in Table I. The overlap functions for these states are compatible with a $\pi/2$ phase shift. However, the computed partial widths do not match those claimed in Ref. [71]: I find 0.51 ± 0.02 MeV to the ^{7}Be ground state versus 0.12 ± 0.04 MeV measured and 0.039 ± 0.002 MeV to the ^{7}Be excited state versus 0.24 ± 0.11 MeV measured. The origin of these differences is not clear.

2. ^{9}He

The spectroscopy of ^{9}He remains unclear despite several experimental studies [85–92]. The ground state was originally thought to be a $1/2^-$ resonance state [85]. Subsequently, strong s-wave n-^{8}He interaction was seen near threshold and was argued to reflect a $1/2^+$ virtual state [86,87]. More recent experiments have revealed a smaller scattering length and thus lend less support to a virtual state [91,92]. Because s-wave neutrons do not have true resonances passing through a $\pi/2$ phase shift, I do not present a width for this state.

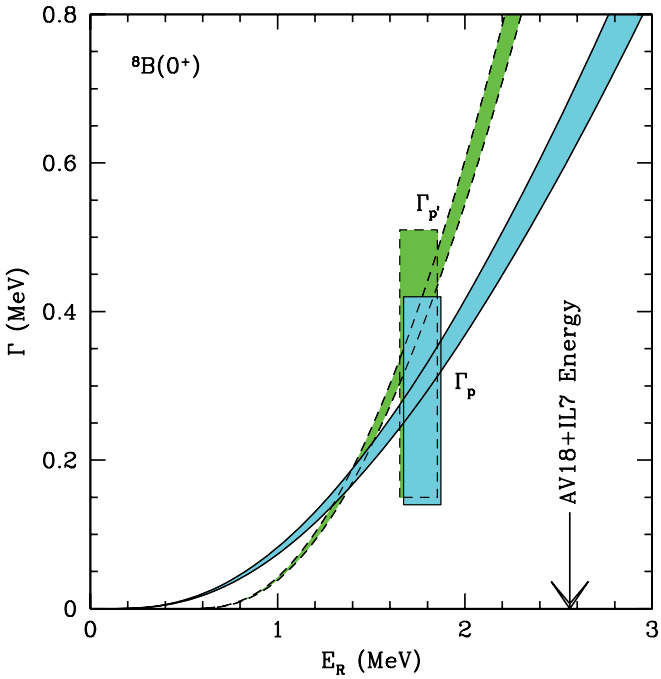

FIG. 6. (Color online) Predicted partial widths as functions of assumed resonance energy (relative to the ^{7}Be ground-state threshold) for the first 0^+ state in ^{8}B. The thicknesses of the bands indicate the errors from Monte Carlo sampling. The band bounded by solid curves indicates the partial width to the ground state of ^{7}Be, and that bounded by dashed curves shows the partial width to the first excited state. The boxes (offset from each other slightly in the horizontal direction for visibility) show the experimental results of Ref. [71] without a correction from R-matrix formal width to observed width. (This can amount to a ∼30% reduction at the high end of the allowed width.) Also indicated is the best estimate of the resonance energy from GFMC calculations using the AV18 + IL7 Hamiltonian.

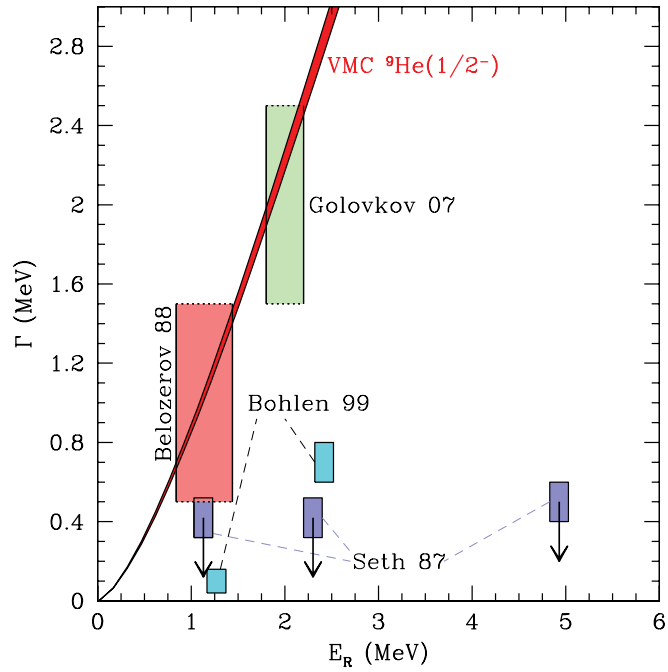

FIG. 7. (Color online) Reported and computed ^{9}He resonance widths. Resonances for which there are reported widths are shown as boxes, with sizes indicating reported errors. The band labeled "VMC" shows the predicted width of the $1/2^-$ state as a function of the resonance energy assumed in the integral relation, and its width reflects the statistical error of the Monte Carlo integration. Where no error was reported for a width (for example, Ref. [91] has "∼2 MeV" for the width of the state at 2.0 MeV), I have assigned an error of 0.5 MeV and indicated this with broken lines at the upper and lower limits. I have omitted some very broad states with missing or lower-limit errors: a state with $E_R \sim 3$ MeV and $\Gamma \sim 3$ MeV from Ref. [93] and one with $E_R \geqslant 4.2$ MeV and $\Gamma > 0.5$ MeV from Ref. [91]. See Ref. [92] for additional reports of states without measured widths. The displayed widths are from Seth *et al.* [85], Belozerov *et al.* [93], Bohlen *et al.* [86], and Golovkov *et al.* [91]. Downward arrows indicate widths that include ∼400 keV instrumental resolution.

Several other observations of resonances within a few MeV of the ^{8}He + n "threshold" have been claimed. (See Ref. [92] for a summary.) Spin and parity assignments for all of these states are uncertain, and matching them to theoretical expectations has proven difficult [68,87,89]. Width estimates based on *ab initio* calculations could provide useful guidance, so I explore this possibility here.

There have been four claims of a state around 1.2 MeV above the ^{8}He + n "threshold" [85,86,92,93], and it has additional support from a study of possible analog states [88]. This is generally assumed to be the lowest-lying p-shell state, with $J^\pi = 1/2^-$, and there is conflicting information concerning its width. The authors of Ref. [85] found it to be narrower than their 0.42-MeV resolution; other experiments gave 1 MeV [93], 0.10 ± 0.06 MeV [86], and 2 MeV [91]. As pointed out particularly by Barker [89], it is difficult to reconcile widths considerably narrower than 1 MeV with the expected strong single-particle character of the $1/2^-$ resonance. Theoretical calculations also place the $1/2^-$ state a few MeV higher (e.g., at 3 and 4 MeV in GFMC calculations with Illinois-6 and Illinois-2 three-body forces, respectively). One possibility is reduction of the $1/2^-$ energy by an sd-shell component that is missing in the calculations [19].

Additional resonances have been found at higher energies: one around 2.3 MeV [85,86,92] with claimed width 0.7 ± 0.2 MeV, one around 4 MeV [86,91], and another around 5 MeV [85,86]. In addition to the $1/2^-$ state, a $3/2^-$ state is expected theoretically, though also at higher energy. It is also likely that sd-shell intruder states with $J^\pi = 5/2^+$ and $3/2^+$ are present in the low-lying spectrum.

I computed widths of p-shell states with $J^\pi = 1/2^-$ and $3/2^-$, but the results proved difficult to match with experimental data. The short-range overlaps of the $1/2^-$ state computed directly and by the integral method are in nice agreement. Since it is unclear what resonance energy should be used in the calculation, I have computed widths from the VMC wave function using a range of channel energies in the integral relation. Figure 7 shows these results. They mainly demonstrate the argument of Barker [89] that there is a mismatch between the narrow width of the $1/2^-$ state claimed by Bohlen *et al.* [86] and theoretical expectations of a strongly single-particle state. The resonances claimed by Belozerov *et al.* [93] and Golovkov *et al.* [91] are consistent

with the computed $1/2^-$ width, but that assignment makes interpretation of the 1.3- and 2.4-MeV states of Bohlen *et al.* [86] difficult: at least one would have to be an sd-shell state.

All channel energies below 6 MeV for the $3/2^-$ state yield computed widths of less than 5 keV. This could match either of the states at 4.3 and 5.3 MeV in Ref. [86], which were found to be narrower than the 100-keV experimental resolution, but the VMC overlaps of this state are inconsistent with $\pi/2$ phase shift. For this reason, the integral-relation results are probably not reliable predictions of the width.

VMC wave functions also exist for states with $J^\pi = 1/2^+$, $3/2^+$, and $5/2^+$, but these wave functions with sd-shell components have not reached the same level of development as the VMC p-shell states and have not been published. As mentioned above, the $1/2^+$ state should not be observable as a resonance. The VMC wave functions for the $3/2^+$ and $5/2^+$ states indicate that they are mainly made by coupling the 2^+ state of ^{8}He to an s-wave neutron and therefore are also not true $\delta_a = \pi/2$ resonances. I did not attempt calculations of partial widths for decay to the ^{8}He(2^+) state. Calculations of the partial widths for decay from positive-parity states to the ^{8}He ground state by emission of a d-wave neutron yielded partial widths of less than 60 keV and overlaps inconsistent with a $\pi/2$ phase shift.

3. ^{9}Li

The most recent data compilation for $A = 9$ lists five low-lying states of ^{9}Li, and firm spins and parities are only assigned to the lowest two [68]. In a more recent paper [63] the third state has been identified as $J^\pi = 5/2^-$ by comparing spectroscopic factors of VMC wave functions (older versions of those used here) with measured (d, p) cross sections. Those authors also assigned $J^\pi = 3/2^-$ and $7/2^-$, respectively, to the next two states. This assignment was based partly on the ordering of states in theoretical calculations and partly on the assumption that widths should correlate with computed spectroscopic factors. The results presented in Table I and Fig. 3 support these assignments by reproducing the widths of all three unbound states.

D. Comparison with other width estimates

I conclude by considering other ways to estimate widths from VMC wave functions and comparing them with the integral method. In the absence of integral relations or explicit scattering calculations, widths must be estimated from spectroscopic factors. In applications of the shell model, one often assumes that the width is the product of the spectroscopic factor,

$$S_a \equiv \int_0^\infty [R_a(r)]^2 r^2\, dr, \tag{53}$$

and the single-particle width. VMC spectroscopic factors might in fact be more suited to this procedure than those from a shell model, because shell models are typically confined to a single value of the principal quantum number, while the large amount of correlation in VMC wave functions guarantees that Eq. (18) picks up contributions from all major shells.

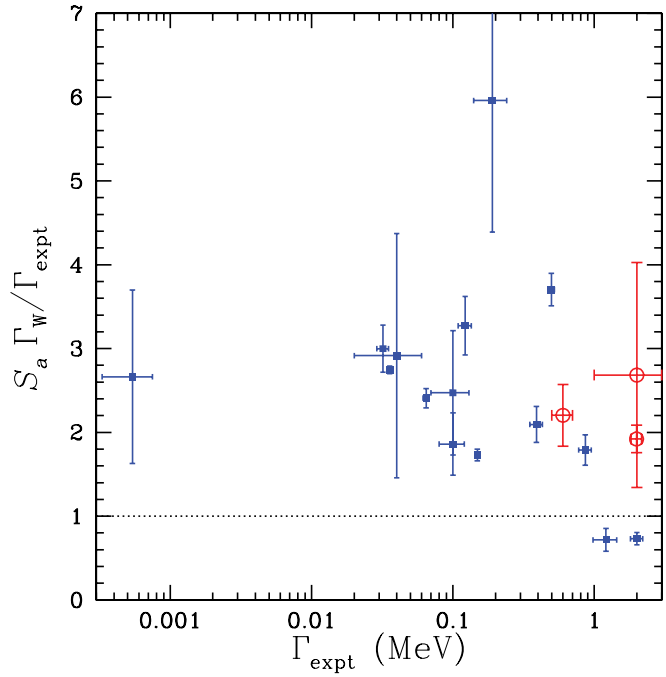

FIG. 8. (Color online) Comparison between experimental widths and widths estimated as the VMC spectroscopic factor times the Wigner limit. The vertical axis shows the ratio of these numbers, using a radius of 4 fm to compute the Wigner limit. Symbols are as in Fig. 3, and the labels from that figure may be used to identify states here. Comparison with Fig. 3 indicates that the integral relation is a significantly better predictor of widths than $S_a\Gamma_W$. Note the different vertical scale from that of Fig. 3.

The crudest estimate of the single-particle width is the "Wigner limit" [94]. On the basis of a causality argument, the width of a resonance can be shown to have an approximate upper limit of

$$\Gamma_W = 2\frac{\hbar^2}{\mu_a b^2} P_l(k_a b), \tag{54}$$

where b is a "matching radius" (typically $\sim$4 fm) defining the edge of the interaction region, and P_l is the penetration factor of Ref. [40]. Since Γ_W is (approximately) an upper limit on the width that a resonance can have, it might approximate a single-particle width. Some authors define Γ_W to include an additional numerical factor multiplying Eq. (54), reflecting assumptions about the wave function inside the interaction region. Teichmann and Wigner [94] assumed a constant wave function to arrive at a factor of $3/2$. Other authors make more elaborate assumptions and arrive at a factor of $(2l-1)/(2l+1)$ for $l \neq 0$ [95]. I take Eq. (54) to define Γ_W.

In Fig. 8 I use the Wigner limit to estimate widths of the states under consideration. In each case, I multiply Γ_W for a 4-fm radius by the VMC spectroscopic factor from Eqs. (18) and (53). These estimates plainly do not reproduce measured widths as well as the integral relation. The weighted mean ratio of "theoretical" to experimental width for this method, restricted to states consistent with $\pi/2$

phase shift and purely nucleon-emission decay, is 2.49 ± 0.52; the reduced χ^2 is 1845 for eight degrees of freedom. (Recall that $\langle \Gamma_{\text{integral}}/\Gamma_{\text{expt}} \rangle = 1.08 \pm 0.04$ with $\chi^2_\nu = 1.6$ for the same set of states.) The mismatch between $S_a\Gamma_W$ and Γ_{expt} can be reduced by choosing a smaller numerical factor to define the Wigner limit, but that does not remove the large scatter in $S_a\Gamma_W/\Gamma_{\text{expt}}$. Better agreement with experiment is likewise achieved with a smaller radius, but good agreement requires an unphysically small radius in the neighborhood of 2 fm, which again does not remove the large scatter in the ratio $S_a\Gamma_W/\Gamma_{\text{exp}}$. Estimates from Γ_W are typically ∼20% smaller if they are estimated as "observed widths" from Eq. (51), using

$$\gamma_a^2 = S_a \frac{\hbar^2}{\mu_a b^2}. \tag{55}$$

This helps significantly with neither the overall scale nor the large scatter of the predicted widths.

A better estimate of the single-particle width, and one perhaps more widespread in shell-model studies, is based on Woods-Saxon potentials. One assumes a potential well of "standard" radius and diffuseness and adjusts its depth to produce a resonance at the correct energy. The width Γ_{WS} of this resonance is then taken as an estimate of the single-particle width. A range of geometric parameters for the potential is usually considered, because the most appropriate values are not known *a priori*.

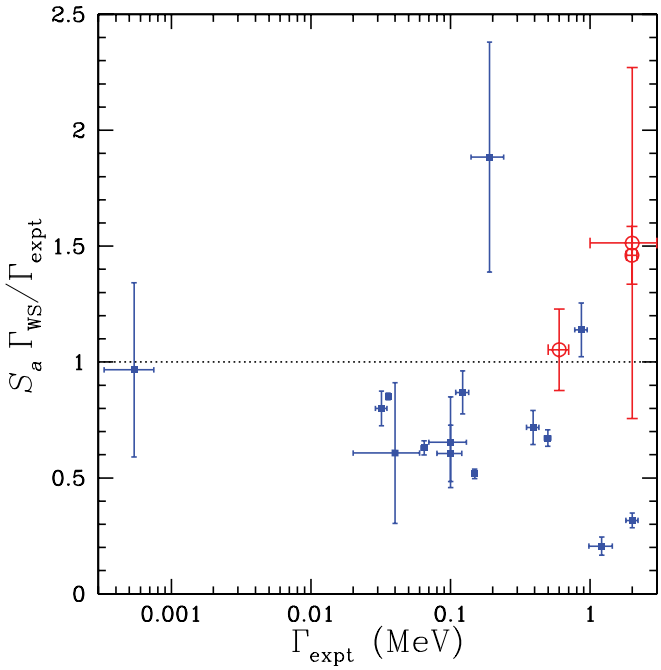

FIG. 9. (Color online) Widths estimated as the VMC spectroscopic factor times the Woods-Saxon single-particle width Γ_{WS}, divided by experimental widths. Symbols are as in Fig. 3, and the labels from that figure may be used to identify states here. Comparison with Figs. 3 and 8 indicates that this approach predicts experimental widths more accurately than the Wigner-limit approach but still not as well as the integral relation.

I computed estimates of this kind, using a diffuseness of 0.65 fm and a Woods-Saxon radius of 1.15 fm $\times (A-1)^{1/3}$, with A the mass number of the resonance state (the defaults in a code provided by Brown [96]). I neglected variation of these parameters and estimated the single-particle width Γ_{WS} from the FWHM of the peak in the computed cross section for the given Woods-Saxon well. The comparison of $S_a\Gamma_{\text{WS}}$ with Γ_{expt} is shown in Fig. 9. The Woods-Saxon estimates are systematically low, with a weighted mean $\langle S_a\Gamma_{\text{WS}}/\Gamma_{\text{expt}} \rangle = 0.74 \pm 0.15$ for the same eight cases considered above and $\chi^2_\nu = 34$ for eight degrees of freedom. I conclude from this exercise and the similar exercise using Wigner limits that VMC widths computed by the integral method are more useful predictors of experimental widths than are the VMC spectroscopic factors.

V. SUMMARY

I have presented plausibility arguments, supported by detailed derivations in the literature, that widths of resonant states can be estimated by evaluating an integral over pseudobound *ab initio* wave functions. This approach is approximate, but it avoids a great deal of computation and human labor that would be needed in full-on scattering calculations and would often be complicated by coupled channels. It is nicely suited to quantum Monte Carlo calculations in that it is insensitive to the difficult-to-compute tails of the many-body wave functions, involves a short-range integral amenable to Monte Carlo integration, uses more information about the Hamiltonian than is encoded in the variational wave function, and can be applied to resonances narrower than the practical energy resolution of the GFMC technique. Related integrals yield overlap functions for bound states, and these overlaps are guaranteed to have the correct shapes in their long-range asymptotics even when the variational wave function does not. These may be useful for calculations of spectroscopic factors and of transfer and knockout cross sections.

I have implemented integral-method width calculations for one-nucleon emission from wave functions computed by the variational Monte Carlo method. It yields widths in good agreement with experiment for several states in the $7 \leqslant A \leqslant 9$ mass range. Cases of disagreement always involve either open channels for which I have not accounted or a resonant wave function that is not strongly peaked in the interaction region. I have shown that widths predicted in this way are closer matches to experiment than are naive combinations of *ab initio* spectroscopic factors with Wigner-limit or Woods-Saxon estimates of single-particle widths. The integral method is thus a useful tool for estimating widths from *ab initio* methods that produce pseudobound wave functions.

For the longer term, the calculations presented here represent a learning problem for application of integrals of the type in Eqs. (32) and (33) to QMC wave functions. Application to GFMC wave functions of the methods used here will be straightforward and mainly involve additional bookkeeping similar to that used in Ref. [60] for direct overlap calculations. Integrals of the kind considered here are likely to find their most extensive use in *ab initio* calculations of coupled-channel

scattering and reactions, and a major goal of the work presented here is to prepare the way for such calculations.

ACKNOWLEDGMENTS

I acknowledge useful discussions with C. A. Bertulani, I. Brida, B. A. Brown, C. R. Brune, H. Esbensen, A. M. Mukhamedzhanov, S. C. Pieper, and J. P. Schiffer. I thank R. B. Wiringa for providing variational wave functions and much guidance in their use. This work was supported by the US Department of Energy, Office of Nuclear Physics, under Contract No. DE-AC02-06CH11357. Calculations were performed on the Fusion computing cluster operated by the Laboratory Computing Resource Center at Argonne.

[1] S. C. Pieper and R. B. Wiringa, Annu. Rev. Nucl. Part. Sci. **51**, 53 (2001).
[2] S. C. Pieper, Riv. Nuovo Cimento **31**, 709 (2008).
[3] P. Navrátil *et al.*, J. Phys. G **36**, 083101 (2009).
[4] R. Roth, T. Neff, H. Hergert, and H. Feldmeier, Nucl. Phys. A **745**, 3 (2004).
[5] R. B. Wiringa and S. C. Pieper, Phys. Rev. Lett. **89**, 182501 (2002).
[6] S. C. Pieper, V. R. Pandharipande, R. B. Wiringa, and J. Carlson, Phys. Rev. C **64**, 014001 (2001).
[7] A. Deltuva, A. C. Fonseca, and P. U. Sauer, Annu. Rev. Nucl. Sci. **58**, 27 (2008).
[8] A. Kievsky, M. Viviani, and L. E. Marcucci, Phys. Rev. C **85**, 014001 (2012).
[9] M. Viviani, A. Deltuva, R. Lazauskas, J. Carbonell, A. C. Fonseca, A. Kievsky, L. E. Marcucci, and S. Rosati, Phys. Rev. C **84**, 054010 (2011).
[10] L. E. Marcucci, A. Kievsky, L. Girlanda, S. Rosati, and M. Viviani, Phys. Rev. C **80**, 034003 (2009).
[11] K. M. Nollett, S. C. Pieper, R. B. Wiringa, J. Carlson, and G. M. Hale, Phys. Rev. Lett. **99**, 022502 (2007).
[12] P. Navrátil, R. Roth, and S. Quaglioni, Phys. Rev. C **82**, 034609 (2010).
[13] P. Navrátil and S. Quaglioni, Phys. Rev. C **83**, 044609 (2011).
[14] P. Navrátil, R. Roth, and S. Quaglioni, Phys. Lett. B **704**, 379 (2011).
[15] P. Navrátil and S. Quaglioni, Phys. Rev. Lett. **108**, 042503 (2012).
[16] G. Hagen, D. J. Dean, M. Hjorth-Jensen, and T. Papenbrock, Phys. Lett. B **656**, 169 (2007).
[17] G. Hagen, T. Papenbrock, and M. Hjorth-Jensen, Phys. Rev. Lett. **104**, 182501 (2010).
[18] G. Gamow, Z. Phys. **51**, 204 (1928).
[19] S. C. Pieper, K. Varga, and R. B. Wiringa, Phys. Rev. C **66**, 044310 (2002).
[20] S. C. Pieper, R. B. Wiringa, and J. Carlson, Phys. Rev. C **70**, 054325 (2004).
[21] S. C. Pieper (private communication).
[22] S. G. Kadmenskiĭ and V. G. Khlebostroev, Sov. J. Nucl. Phys. **18**, 505 (1974) [Yad. Fiz. **18**, 980 (1973)].
[23] V. P. Bugrov and S. G. Kadmenskii, Sov. J. Nucl. Phys. **49**, 967 (1989) [Yad. Fiz. **49**, 1562 (1989)].
[24] S. Åberg, P. B. Semmes, and W. Nazarewicz, Phys. Rev. C **56**, 1762 (1997).
[25] S. Åberg, P. B. Semmes, and W. Nazarewicz, Phys. Rev. C **58**, 3011 (1998).
[26] C. N. Davids *et al.*, Phys. Rev. Lett. **80**, 1849 (1998).
[27] A. A. Sonzogni, C. N. Davids, P. J. Woods, D. Seweryniak, M. P. Carpenter, J. J. Ressler, J. Schwartz, J. Uusitalo, and W. B. Walters, Phys. Rev. Lett. **83**, 1116 (1999).
[28] C. N. Davids and H. Esbensen, Phys. Rev. C **61**, 054302 (2000).
[29] H. Esbensen and C. N. Davids, Phys. Rev. C **63**, 014315 (2000).
[30] A. M. Mukhamedzhanov and N. K. Timofeyuk, Sov. J. Nucl. Phys. **51**, 431 (1990) [Yad. Fiz. **51**, 679 (1990)].
[31] D. R. Lehman and B. F. Gibson, Phys. Rev. C **13**, 35 (1976).
[32] M. Viviani, A. Kievsky, and S. Rosati, Phys. Rev. C **71**, 024006 (2005).
[33] K. M. Nollett and R. B. Wiringa, Phys. Rev. C **83**, 041001 (2011).
[34] P. Barletta, C. Romero-Redondo, A. Kievsky, M. Viviani, and E. Garrido, Phys. Rev. Lett. **103**, 090402 (2009).
[35] Y. Suzuki, W. Horiuchi, and K. Arai, Nucl. Phys. A **823**, 1 (2009).
[36] A. Kievsky, M. Viviani, P. Barletta, C. Romero-Redondo, and E. Garrido, Phys. Rev. C **81**, 034002 (2010).
[37] Y. Suzuki, D. Baye, and A. Kievsky, Nucl. Phys. A **838**, 20 (2010).
[38] C. Romero-Redondo, E. Garrido, P. Barletta, A. Kievsky, and M. Viviani, Phys. Rev. A **83**, 022705 (2011).
[39] M. Abramowitz and I. A. Stegun, *Handbook of Mathematical Functions* (Dover, New York, 1972).
[40] A. M. Lane and R. G. Thomas, Rev. Mod. Phys. **30**, 257 (1958).
[41] E. I. Dolinskii and A. M. Mukhamedzhanov, Bull. Acad. Sci. USSR, Phys. Ser. **41**, 55 (1977) [Izvest. Akad. Nauk SSSR. Ser. Fiz. **41**, 2055 (1977)].
[42] J. Humblet and L. Rosenfeld, Nucl. Phys. **26**, 529 (1961).
[43] J. Okołowicz, N. Michel, W. Nazarewicz, and M. Płoszajczak, Phys. Rev. C **85**, 064320 (2012).
[44] J. Humblet, Nucl. Phys. A **151**, 225 (1970).
[45] J. Humblet, Phys. Rev. C **42**, 1582 (1990).
[46] A. M. Mukhamedzhanov and R. E. Tribble, Phys. Rev. C **59**, 3418 (1999).
[47] L. S. Rodberg and R. M. Thaler, *Introduction to the Quantum Theory of Scattering* (Academic, New York, 1967).
[48] R. G. Newton, *Scattering Theory of Waves and Particles*, 2nd ed. (Dover, Mineola, NY, 1982).
[49] W. Pinkston and R. Satchler, Nucl. Phys. A **72**, 641 (1965).
[50] N. K. Timofeyuk, Nucl. Phys. A **632**, 19 (1998).
[51] J. M. Blatt and J. D. Jackson, Phys. Rev. **76**, 18 (1949).
[52] M. Kawai and K. Yazaki, Prog. Theor. Phys. **37**, 638 (1967).
[53] N. K. Timofeyuk, Phys. Rev. C **81**, 064306 (2010).
[54] J. L. Friar, B. F. Gibson, D. R. Lehman, and G. L. Payne, Phys. Rev. C **37**, 2859 (1988).
[55] R. B. Wiringa, V. G. J. Stoks, and R. Schiavilla, Phys. Rev. C **51**, 38 (1995).
[56] B. S. Pudliner, V. R. Pandharipande, J. Carlson, S. C. Pieper, and R. B. Wiringa, Phys. Rev. C **56**, 1720 (1997).
[57] R. B. Wiringa, AIP Conf. Proc. **1128**, 1 (2009).
[58] R. B. Wiringa, Phys. Rev. C **43**, 1585 (1991).

[59] R. B. Wiringa (private communication).
[60] I. Brida, S. C. Pieper, and R. B. Wiringa, Phys. Rev. C **84**, 024319 (2011).
[61] L. Lapikás, J. Wesseling, and R. B. Wiringa, Phys. Rev. Lett. **82**, 4404 (1999).
[62] A. H. Wuosmaa *et al.*, Phys. Rev. C **72**, 061301 (2005).
[63] A. H. Wuosmaa *et al.*, Phys. Rev. Lett. **94**, 082502 (2005).
[64] S. C. Pieper, in *New Facet of Three Nucleon Force—50 Years of Fujita Miyazawa*, edited by H. Sakai, K. Sekiguchi, and B. F. Gibson, Vol. 1011 of AIP Conference Series (American Institute of Physics, Melville, NY, 2008), pp. 143–152.
[65] M. Pervin, S. C. Pieper, and R. B. Wiringa, Phys. Rev. C **76**, 064319 (2007).
[66] L. E. Marcucci, M. Pervin, S. C. Pieper, R. Schiavilla, and R. B. Wiringa, Phys. Rev. C **78**, 065501 (2008).
[67] D. R. Tilley, C. M. Cheves, J. L. Godwin, G. M. Hale, H. M. Hofmann, J. H. Kelley, C. G. Sheu, and H. R. Weller, Nucl. Phys. A **708**, 3 (2002).
[68] D. R. Tilley, J. H. Kelley, J. L. Godwin, D. J. Millener, J. E. Purcell, C. G. Sheu, and H. R. Weller, Nucl. Phys. A **745**, 155 (2004).
[69] M. Skill, R. Baumann, G. Keil, N. Kniest, E. Pfaff, M. Preiss, G. Reiter, G. Clausnitzer, M. Haller, and W. Kretschmer, Nucl. Phys. A **581**, 93 (1995).
[70] S. F. Mughabghab and D. I. Garber, *Neutron Cross Sections BNL-325*, Vol. I: Resonance Parameters, 3rd. ed. (Brookhaven National Laboratory, Upton, NY, 1973).
[71] J. P. Mitchell, G. V. Rogachev, E. D. Johnson, L. T. Baby, K. W. Kemper, A. M. Moro, P. N. Peplowski, A. Volya, and I. Wiedenhöver, Phys. Rev. C **82**, 011601 (2010).
[72] Y. S. Chen, T. A. Tombrello, and R. W. Kavanagh, Nucl. Phys. A **146**, 136 (1970).
[73] S. Dixit *et al.*, Phys. Rev. C **43**, 1758 (1991).
[74] G. Audi, A. H. Wapstra, and C. Thibault, Nucl. Phys. A **729**, 337 (2003).
[75] E. Teranishi and B. Furubayashi, Phys. Lett. **9**, 157 (1964).
[76] W. Benenson and E. Kashy, Phys. Rev. C **10**, 2633 (1974).
[77] H. G. Bohlen, R. Kalpakchieva, A. Blažević, B. Gebauer, T. N. Massey, W. von Oertzen, and S. Thummerer, Phys. Rev. C **64**, 024312 (2001).
[78] R. H. Stokes and P. G. Young, Phys. Rev. **178**, 2024 (1969).
[79] A. H. Wuosmaa *et al.*, Phys. Rev. C **78**, 041302 (2008).
[80] R. L. McGrath, J. Cerny, and E. Norbeck, Phys. Rev. Lett. **19**, 1442 (1967).
[81] J. C. Adloff, K. H. Souw, and C. L. Cocke, Phys. Rev. C **3**, 1808 (1971).
[82] F. C. Barker and N. Ferdous, Aust. J. Phys. **31**, 239 (1978).
[83] F. C. Barker, Aust. J. Phys. **31**, 27 (1978).
[84] M. A. Oothoudt and G. T. Garvey, Nucl. Phys. A **284**, 41 (1977).
[85] K. K. Seth, M. Artuso, D. Barlow, S. Iversen, M. Kaletka, H. Nann, B. Parker, and R. Soundranayagam, Phys. Rev. Lett. **58**, 1930 (1987).
[86] H. Bohlen, A. Blazevicá, B. Gebauer, W. V. Oertzen, S. Thummerer, R. Kalpakchieva, S. Grimes, and T. Massey, Prog. Part. Nucl. Phys. **42**, 17 (1999).
[87] L. Chen, B. Blank, B. A. Brown, M. Chartier, A. Galonsky, P. G. Hansen, and M. Thoennessen, Phys. Lett. B **505**, 21 (2001).
[88] G. V. Rogachev *et al.*, Phys. Rev. C **67**, 041603 (2003).
[89] F. C. Barker, Nucl. Phys. A **741**, 42 (2004).
[90] A. Volya and V. Zelevinsky, Phys. Rev. Lett. **94**, 052501 (2005).
[91] M. S. Golovkov *et al.*, Phys. Rev. C **76**, 021605 (2007).
[92] H. T. Johansson *et al.*, Nucl. Phys. A **842**, 15 (2010).
[93] A. V. Belozerov, K. Borcza, Z. Diougy, A. M. Kalinin, H. T. Nguyen, and Y. E. Penionzhkevich, Bull. Sov. Acad. Sci., Phys. Ser. **52**, 94 (1988) [Izv. Akad. Nauk USSR Phys. Ser. **52**(1), 100 (1988)].
[94] T. Teichmann and E. P. Wigner, Phys. Rev. **87**, 123 (1952).
[95] A. Bohr and B. R. Mottelson, *Nuclear Structure*, Vol. 1 (Benjamin, New York, 1969).
[96] B. A. Brown (private communication).